We also found that TPA long term treatment down-regulated the phosphorylated levels of PKCα/β, PKCε and PKCδ compared with those in these cells without TPA (Fig. 3D).

Effect of OAG on the HSP27 phosphorylation in HuH7 cells

OAG, a synthetic diacylglycerol (DAG), which is generally recognized to be a physiological activator of PKC (Nishizuka, 1991; Schutze et al., 1991), strengthened the phosphorylated levels of HSP27 in a time-dependent manner (Fig. 4A) as well as TPA. The phosphorylated levels reached its peak at 10 min after the stimulation and decreased thereafter (Fig. 4A). We next examined the effect of bisindolylmaleimide I on OAG-induced levels of HSP27 phosphorylation. Bisindolylmaleimide I (30 μM) suppressed OAG-induced phosphorylated levels of HSP27 (Fig. 4B). In addition, OAG-induced phosphorylation of novel PKC(δ, ε) was also suppressed by bisindolylmaleimide I (Fig. 4C).

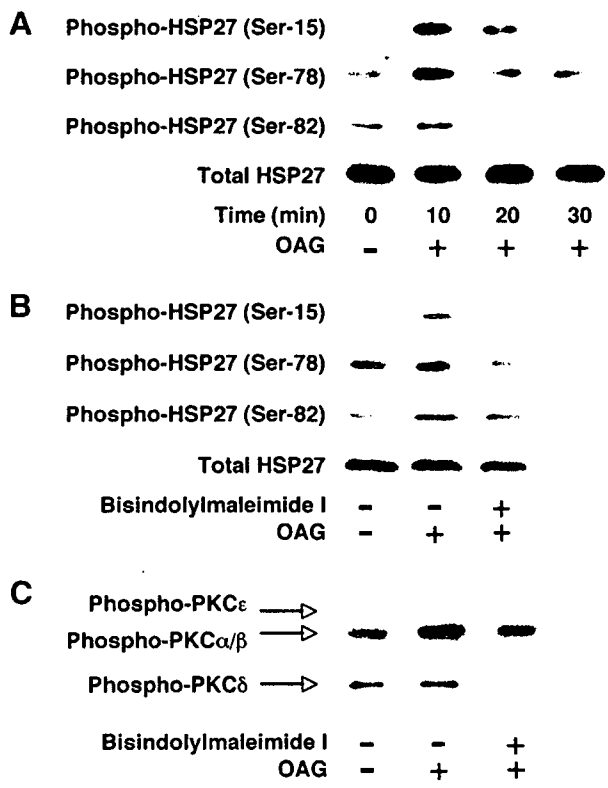

Fig. 4. Effect of OAG on the phosphorylation of HSP27, and effects of bisindorylmaleimide I on the OAG-induced HSP27 phosphorylation and PKC phosphorylation in HuH7 cells. HuH7 cells were cultured in DMEM containing 10% FCS for 7 days. After 7 days, the medium was exchanged for FCS-free DMEM. The cells were immediately used for experiments. (A) The cultured cells were stimulated with 100 μM OAG for the indicated periods. (B, C) The cultured cells were pre-treated with 30 μM of bisindorylmaleimide I or vehicle for 60 min, and then stimulated with 100 μM OAG or vehicle for 10 min. The extracts of cells were subjected to SDS-PAGE with subsequent Western blotting analysis with antibodies against (A, B) phospho-HSP27 (Ser-15), phospho-HSP27 (Ser-78), phospho-HSP27 (Ser-82) and total HSP27, and (C) phospho-PKC (pan) (βII Ser-660) and phospho-PKCδ (Thr-505). Representative results from triplicate independent experiments with similar results are shown.

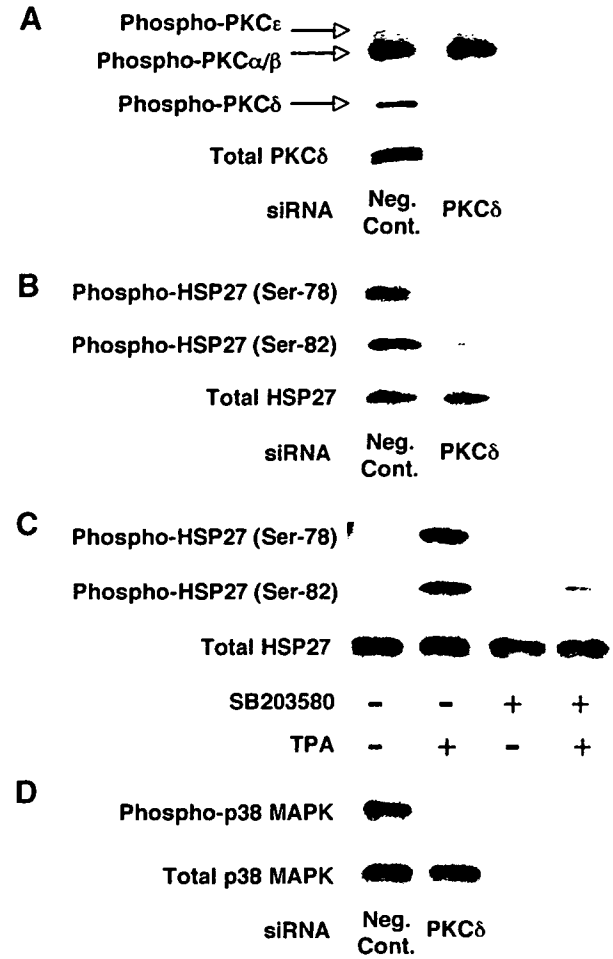

Fig. 5. Effect of gene silencing using PKCδ-siRNA-transfection into HuH7 cells and effect of SB203580 on the TPA-induced HSP27 phosphorylation in HuH7 cells. (A, B, D) HuH7 cells were cultured in DMEM containing 10% FCS for 24 h. After 24 h, the cells were incubated with 10 nM of PKCδ siRNA or negative control siRNA at 37 °C for 48 h in DMEM containing 10% FCS and subsequently harvested for preparation of Western blotting analysis. (C) HuH7 cells were cultured in DMEM containing 10% FCS for 7 days. After 7 days, the medium was exchanged for FCS-free DMEM. The cells were immediately used for experiments. The cultured cells were pre-treated with 30 μM of SB203580 or vehicle for 60 min and then, stimulated by 0.1 μM TPA or vehicle for 60 min. The extracts of cells were subjected to SDS-PAGE with subsequent Western blotting analysis with antibodies against (A) phospho-PKC (pan) (βII Ser-660), phospho-PKCδ (Thr-505) and total PKCδ, (B, C) phospho-HSP27 (Ser-78), phospho-HSP27 (Ser-82) and total HSP27, and (D) phospho-p38 MAPK and total p38 MAPK. The total PKCδ antibody confirms silencing of PKCδ protein expression, and total HSP27 antibody is used to control for loading and specificity of PKCδ siRNA. Representative results from triplicate independent experiments with similar results are shown. Neg. Cont.: negative control.

Effect of gene silencing using PKCδ-siRNA- or PKCε-siRNA-transfection into HuH7 cells

Based on our findings, it is probable that phosphorylation of HSP27 is regulated by activation of novel PKC. To clarify which isoform of novel PKC acts in the phosphorylation of HSP27 in HuH7 cells, we examined the effect of gene silencing using PKCδ-siRNA-transfection into HuH7 cells. We found that PKCδ knock down selectively decreased expression of

PKCδ (Fig. 5A). In PKCδ-knocked down HuH7 cells, the phosphorylated levels of HSP27 were much reduced, while expression levels of total HSP27 were not changed (Fig. 5B). In addition, we examined the effect of gene silencing using PKCε-siRNA-transfection into HuH7 cells. However, both phosphorylated levels of HSP27 and expression levels of total HSP27 were not changed in PKCε-knocked down HuH7 cells (data not shown).

Effect of SB203580 on TPA-induced HSP27 phosphorylation

It is well-recognized that HSP27 is phosphorylated at serines 15, 78, and 82 by MAPKAP kinase 2 as a result of p38 MAPK pathway activation (Landry et al., 1992; Rouse et al., 1994). In contrast, a recent study showed that PKCδ directly binds to HSP27 and induces HSP27 phosphorylation (Lee et al., 2005). To determine whether p38 MAPK is involved in PKCδ-mediated HSP27 phosphorylation in HuH7 cells, we next investigated the effect of SB203580 (Cuenda et al., 1995), a specific inhibitor of p38 MAPK on TPA-induced HSP27 phosphorylation. SB203580 (30 μM) almost completely suppressed TPA-induced phosphorylation of HSP27 (Fig. 5C).

To clarify whether PKCδ exerts its effect at upstream of p38 MAPK activation, we examined the effect of gene silencing of PKCδ by siRNA into HuH7 cells. PKCδ knock down markedly suppressed phosphorylation of p38 MAPK in these cells (Fig. 5D).

Discussion

It has been shown that phosphorylation of HSP27 is mediated by the MAPK superfamily (Kyriakis and Avruch, 1996; Guay et al., 1997; Benjamin and McMillan, 1998). Although p44/p42 MAPK is highly activated in HCC (Ito et al., 1998; Iyoda et al., 2003), we demonstrated that phosphorylation of HSP27 was not correlated with p44/p42 MAPK activity. It has been reported that PKC is an upstream regulator of the MAPK superfamily cascade (Noguchi et al., 1993; Tanaka et al., 2003; Tokuda et al., 2003). Therefore, we examined whether PKC regulates the HSP27 phosphorylation in HCC cells. As expected, we found that the inhibition of PKC with bisindorylmaleimide I, and PKC down-regulation suppressed the basal level of HSP27 phosphorylation in HuH7 cells consistently with the previous reports (Faucher et al., 1993). In addition, the activation of PKC induced by TPA or OAG markedly strengthened HSP27 phosphorylation in HuH7 cells. Although, bisindolylmaleimide I does not seem nearly as effective as an inhibitor of HSP27 phosphorylation prior to OAG (Fig. 4B), when compared to TPA (Fig. 3A), particularly at Ser-15 and Ser-82. TPA, a phorbol ester, is known to activate PKC in an irreversible manner (Nishizuka, 1986). On the other hand, OAG is a physiological activator of PKC (Nishizuka, 1991; Schutze et al., 1991). Therefore, the effect of OAG to induce HSP 27 (shown in Fig. 4B, lane 2) was weaker than that of TPA (shown in Fig. 3A, lane 2), leading to the relative up-regulation of the band (Fig. 4B, lane 3) which shows the inhibitory effect of bisindolylmaleimide I on the OAG-induced HSP27 phosphorylation. Collectively, these findings suggest that PKC might have a pivotal role in the HSP27 phosphorylation in human HCC.

The importance of PKC signaling in tumor cells is corroborated by investigations that characterized the roles of individual PKC isoforms in cell growth regulation and transformation (Hofmann, 1997; Mackay and Twelves, 2003). Since atypical PKC is insensitive to TPA (Nishizuka, 1991), our findings made us to speculate that classical PKC and novel PKC are the candidate for the regulator of HSP27 phosphorylation in HuH7 cells. In the present study, PKCδ and PKCε were phosphorylated by TPA-stimulation and suppressed with bisindorylmaleimide I. In contrast PKCα/β were constitutively activated in HuH7 cells, and were not affected or were at least in part slightly enhanced by both TPA or bisindorylmaleimide I. Furthermore, PKCδ knock down significantly suppressed HSP27 phosphorylation in HuH7 cells. Taking these findings into account, it is most likely that activation of PKCδ regulates the phosphorylation of HSP27 in human HCC.

It is well-recognized that the MAPK cascade, in particular p38 MAPK, phosphorylates HSP27 via MAPK-activated protein kinase-2 (MAPKAPK-2), one of the substrates of p38 MAPK (Landry et al., 1992; Rouse et al., 1994; Guay et al., 1997). While, it has recently been reported that PKCδ directly binds to and phosphorylates HSP27 (Lee et al., 2005). Therefore, we next investigated whether p38 MAPK is involved in PKCδ-mediated HSP27 phosphorylation in HuH7 cells. We showed here that PKCδ knock down resulted in the suppression of p38 MAPK phosphorylation. In addition, we found that SB203580 significantly reduced the levels of HSP27 phosphorylation. Therefore, it is most likely that PKCδ mainly regulates HSP27 phosphorylation at a point upstream of p38 MAPK in human HCC.

Recent evidence suggests that PKCδ acts as a pro-apoptotic, tumor-suppressive molecule (Hofmann, 1997; Mackay and Twelves, 2003; Steinberg, 2004). Unlike PKCβ (which stimulates growth) and PKCε (which acts as an oncogene when over-expressed in rat fibroblasts and promotes tumors in nude mice), PKCδ generally slows the proliferation, induces the cell cycle arrest, and/or enhances the differentiation of various undifferentiated cell lines (Steinberg, 2004). In addition, it has been reported that a PKCδ/p38 MAPK pathway mediates the pro-apoptotic effects in prostate cancer cells (Tanaka et al., 2003). Our present findings seem to be in accordance with these previous observations.

Although the role of phosphorylated HSP27 is not elucidated, it has been reported that p38 MAPK-mediated phosphorylation of HSP27 increases its association with IκB kinase complex to suppress TNF-mediated NF-κB activation (Park et al., 2003). In a previous study (Yasuda et al., 2005), we showed that attenuated phosphorylation of HSP27 correlates with the tumor progression in patients with HCC, i.e. the larger tumors exhibited lower levels of phosphorylated HSP27 than did the smaller tumors. In addition, it has been reported that the activation of p38 MAPK is inversely correlated with the tumor progression in patients with HCC (Iyoda et al., 2003). Based on these findings, it is speculated that PKCδ may prevent tumor progression through phosphorylation of HSP27. Further investigations would be required to clarify the detailed mechanism of

HSP27 phosphorylation and the role of phosphorylated HSP27 in human HCC.

In conclusion, our present results strongly suggest that PKCδ functions as an important regulator in the phosphorylation of HSP27 via p38 MAPK in human HCC.

References

Alessi, D.R., Cuenda, A., Cohen, P., Dulley, D.T., Sartiel, A.R., 1995. PD 098059 is a specific inhibitor of the activation of mitogen-activated protein kinase kinase in vitro and in vivo. Journal of Biological Chemistry 270, 27484–27494.

Arrigo, A.P., 1990. Tumor necrosis factor induces the rapid phosphorylation of the mammalian heat shock protein hsp28. Molecular and Cellular Biology 10, 1276–1280.

Benjamin, I.J., McMillan, D.R., 1998. Stress (heat shock) proteins molecular chaperones in cardiovascular biology and disease. Circulation Research 83, 117–132.

Blumberg, P.M., 1991. Complexities of the protein kinase C pathway. Molecular Carcinogenesis 4, 339–344.

Cuenda, A., Rouse, J., Doza, Y.N., Meier, R., Cohen, P., Gallagher, T.F., Young, R.R., Lee, J.C., 1995. SB203580 is a specific inhibitor of a MAP kinase homologue which is stimulated by cellular stresses and interleukin-1. FEBS Letters 364, 229–233.

Faucher, C., Capdevielle, J., Canal, I., Ferra, P., Mazarguli, H., McGuire, W.L., Darbon, J.M., 1993. The 28-kDa protein whose phosphorylation is induced by protein kinase C activators in MCF-7 cells belongs to the family of low molecular mass heat shock proteins and is the estrogen-regulated 24-kDa protein. Journal of Biological Chemistry 268, 15168–15173.

Geum, D., Son, G.H., Kim, K., 2002. Phosphorylation-dependent cellular localization and thermoprotective role of heat shock protein 25 in hippocampal progenitor cells. Journal of Biological Chemistry 277, 19913–19921.

Guay, J., Lambert, H., Gingras-Breton, G., Lavoie, J.N., Huot, J., Landry, J., 1997. Regulation of actin filament dynamics by p38 MAP kinase-mediated phosphorylation of heat shock protein 27. Journal of Cell Science 110, 357–368.

Hofmann, J., 1997. The potential for isoenzyme-selective modulation of protein kinase C. FASEB Journal 11, 649–669.

Ikeda, K., Saitoh, S., Koida, I., Arase, Y., Tsubota, A., Chayama, K., Kumada, H., Kawanishi, M., 1993. A multivariate analysis of risk factor for hepatocellular carcinogenesis: a prospective observation of 795 patients with viral and alcoholic cirrhosis. Hepatology 18, 47–53.

Ito, Y., Sasaki, Y., Horimoto, M., Wada, S., Tanaka, Y., Kasahara, A., Ueki, T., Hirano, T., Yamamoto, H., Fujimoto, J., Okamoto, E., Hayashi, N., Hori, M., 1998. Activation of mitogen-activated protein kinases/extracellular signal-regulated kinases in human hepatocellular carcinoma. Hepatology 27, 951–958.

Iyoda, K., Sasaki, Y., Horimoto, M., Toyama, T., Yakushijin, T., Sakakibara, M., Takehara, T., Fujimoto, J., Hori, M., Wands, J.R., Hayashi, N., 2003. Involvement of the p38 mitogen-activated protein kinase cascade in hepatocellular carcinoma. Cancer 97, 3017–3026.

Kato, K., Ito, H., Hasegawa, K., Inaguma, Y., Kozawa, O., Asano, T., 1996. Modulation of the stress-induced synthesis of hsp27 and aB-crystallin by cyclic AMP in C6 glioma cells. Journal of Neurochemistry 66, 946–950.

Keranen, L.M., Dutil, E.M., Newton, A.C., 1995. Protein kinase C is regulated in vivo by three functionally distinct phosphorylations. Current Biology 5, 1394–1403.

Koda, M., Murawaki, Y., Mitusda, A., Horie, Y., Suou, T., Kawasaki, H., Ikawa, S., 2000. Predictive factors for intrahepatic recurrence after percutaneous ethanol injection therapy for small hepatocellular carcinoma. Cancer 88, 529–537.

Kumada, T., Nakano, S., Takeda, I., Sugiyama, K., Osada, T., Kiriyama, S., Sone, Y., Toyoda, H., Shimada, S., Takahashi, M., Sassa, T., 1997. Patterns of recurrence after initial treatment in patients with small hepatocellular carcinoma. Hepatology 25, 87–92.

Kyriakis, J.M., Avruch, J., 1996. Sounding the alarm: protein kinase cascades activated by stress and inflammation. Journal of Biological Chemistry 271, 24313–24316.

Laemmli, U.K., 1970. Cleavage of structural proteins during the assembly of the head of bacteriophage T4. Nature 227, 680–685.

Landry, J., Lambert, H., Zhou, M., Lavoie, J.N., Hickey, E., Weber, L.A., Anderson, C.W., 1992. Human HSP27 is phosphorylated at serines 78 and 82 by heat shock and mitogen-activated kinases that recognize the same amino acid motif as S6 kinase II. Journal of Biological Chemistry 267, 794–803.

Lee, Y.J., Lee, D.H., Cho, C.K., Bae, S., Jhon, G.I., Lee, S.J., Soh, J.W., Lee, Y. S., 2005. HSP25 inhibits protein kinase C delta-mediated cell death through direct interaction. Journal of Biological Chemistry 280, 18108–18119.

Mackay, H.J., Twelves, C.J., 2003. Protein kinase C: a target for anticancer drugs? Endocrine-Related Cancer 10, 389–396.

Maizels, E.T., Peters, C.A., Kline, M., Cutler Jr., R.E., Shanmugam, M., Hunzicker-Dunn, M., 1998. Heat-shock protein-25/27 phosphorylation by the delta isoform of protein kinase C. Biochemical Journal 332 (Pt 3), 703–712.

Nishizuka, Y., 1991. Studies and perspectives of protein kinase C. Science 233, 305–312.

Noguchi, T., Metz, R., Chen, L., Mattei, M.G., Carrasco, D., Bravo, R., 1993. Structure, mapping, and expression of erp, a growth factor-inducible gene encoding a nontransmembrane protein tyrosine phosphatase, and effect of ERP on cell growth. Molecular and Cellular Biology 13, 5195–5205.

Park, K.J., Gaynor, R.B., Kwak, Y.T., 2003. Heat shock protein 27 association with I kappa B kinase complex regulates tumor necrosis factor alpha-induced NF-kappa B activation. Journal of Biological Chemistry 278, 35272–35278.

Rouse, J., Cohen, P., Trigon, S., Morange, M., Alonso-Llamazares, A., Zamanillo, D., Hunt, T., Nebreda, A.R., 1994. A novel kinase cascade triggered by stress and heat shock that stimulates MAPKAP kinase-2 and phosphorylation of the small heat shock proteins. Cell 78, 1027–1037.

Saito, K., Kikkawa, U., Nishizuka, Y., 2001. The family of protein kinase C and membrane lipid mediators. Diabetes Complications 16, 4–8.

Schutze, S., Berkovic, D., Tomsing, O., Unger, C., Kronke, M., 1991. Tumor necrosis factor induces rapid production of 1¢2¢diacylglycerol by a phosphatidylcholine-specific phospholipase C. Journal of Experimental Medicine 174, 975–988.

Shiratori, Y., Yoshida, H., Omata, M., 2001. Different clinicopathological features of hepatocellular carcinoma in relation to causative agents. Journal of Gastroenterology 37, 73–78.

Shimada, M., Takenaka, K., Taguchi, K., Fujiwara, Y., Kajiyama, K., Maeda, T., Shirabe, K., Yanaga, K., Sugimachi, K., 1998. Prognostic factors after repeat hepatectomy for recurrent hepatocellular carcinoma. Annals of Surgery 227, 80–85.

Steinberg, S.F., 2004. Distinctive activation mechanism and function for protein kinase Cd. Biochemical Journal 384, 449–459.

Tanaka, Y., Gavrielides, M.V., Mitsuuchi, Y., Fujii, T., Kazanietz, M.G., 2003. Protein kinase C promotes apoptosis in LNCaP prostate cancer cells through activation of p38 MAPK and inhibition of the Akt survival pathway. Journal of Biological Chemistry 278, 33753–33762.

Tokuda, T., Harada, A., Hirade, K., Matsuno, H., Ito, H., Kato, K., Oiso, Y., Kozawa, O., 2003. Incadronate amplifies prostaglandin F2 alpha-induced vascular endothelial growth factor synthesis in osteoblasts. Enhancement of MAPK activity. Journal of Biological Chemistry 278, 18930–18937.

Toullec, D., Pianetti, P., Coste, H., Bellevergue, P., Grand-Perret, T., Ajakane, M., Baudet, V., Boissin, P., Boursier, E., Loriolle, L., Duhamel, L., Charon, D., Kirlowsky, J., 1991. The bisindolylmaleimide GF 109203X is a potent and selective inhibitor of protein kinase C. Journal of Biological Chemistry 266, 15771–15781.

Welch, W.J., 1985. Phorbol ester, calcium ionophore, or serum added to quiescent rat embryo fibroblast cells all result in the elevated phosphorylation of two 27,000-dalton mammalian stress proteins. Journal of Biological Chemistry 260, 3058–3062.

Yasuda, E., Kumada, T., Takai, S., Ishisaki, A., Noda, T., Matsushima-Nishiwaki, R., Yoshimi, N., Kato, K., Toyoda, H., Kaneoka, Y., Yamagichi, A., Kozawa, O., 2005. Attenuated phosphorylation of heat shock protein 27 correlates with tumor progression in patients with hepatocellular carcinoma. Biochemical Biophysical Research Communications 337, 337–342.

Available online at www.sciencedirect.com
ScienceDirect
Metabolism Clinical and Experimental 56 (2007) 476–483
Metabolism
Clinical and Experimental
www.elsevier.com/locate/metabol

Limitation by p70 S6 kinase of platelet-derived growth factor-BB–induced interleukin 6 synthesis in osteoblast-like MC3T3-E1 cells

Shinji Takai[a], Haruhiko Tokuda[a,b], Yoshiteru Hanai[a,b], Osamu Kozawa[a,*]

[a]*Department of Pharmacology, Gifu University Graduate School of Medicine, Gifu 501-1194, Japan*
[b]*Department of Clinical Laboratory, National Hospital for Geriatric Medicine, National Center for Geriatrics and Gerontology, Obu, Aichi 474-8511, Japan*

Received 17 March 2006; accepted 16 November 2006

Abstract

It has been reported that platelet-derived growth factor–BB (PDGF-BB) stimulates interleukin 6 (IL-6) in osteoblasts. In the present study, we investigated the mechanism of IL-6 synthesis induced by PDGF-BB in osteoblast-like MC3T3-E1 cells. Platelet-derived growth factor–BB time-dependently induced the phosphorylation of p44/p42 mitogen-activated protein (MAP) kinase, p38 MAP kinase, stress-activated protein kinase/c-*Jun* N-terminal kinase (SAPK/JNK), and p70 S6 kinase. PD98059 (an inhibitor of MAP kinase/extracellular signal-regulated kinase kinase [MEK]), SB203580 (an inhibitor of p38 MAP kinase), or SP600125 (an inhibitor of SAPK/JNK) suppressed the IL-6 synthesis induced by PDGF-BB. Rapamycin, an inhibitor of p70 S6 kinase, significantly enhanced the PDGF-BB–stimulated IL-6 synthesis. The PDGF-BB–induced phosphorylation of p70 S6 kinase was suppressed by rapamycin. Rapamycin failed to affect the PDGF-BB–induced phosphorylation of p44/p42 MAP kinase, p38 MAP kinase, or SAPK/JNK. These results strongly suggest that PDGF-BB stimulates IL-6 synthesis through activation of 3 MAP kinases in osteoblasts and that p70 S6 kinase negatively regulates the IL-6 synthesis.

1. Introduction

Interleukin 6 (IL-6) is a pleiotropic cytokine that has important physiologic effects on a wide range of functions such as promoting B-cell differentiation and T-cell activation and inducing acute-phase proteins [1-3]. It is generally recognized that bone metabolism is regulated mainly by 2 functional cells, osteoblasts and osteoclasts, responsible for bone formation and bone resorption, respectively [4]. As for bone metabolism, IL-6 has been shown to stimulate bone resorption and promote osteoclast formation [2,3,5,6]. It has been reported that potent bone resorptive agents such as tumor necrosis factor α and IL-1 stimulate IL-6 synthesis in osteoblasts [5,7,8]. Currently, accumulating evidence indicates that IL-6 secreted from osteoblasts plays a pivotal role as a downstream effector of bone-resorptive agents.

It is well known that platelet-derived growth factor (PDGF) is a mitogenic factor, which mainly acts on connective tissue cells [9,10]. Platelet-derived growth factor occurs as 5 different isoforms [10]. Platelet-derived growth factor isoforms were originally isolated from platelets but have been shown to be produced and released from a variety of cell types including osteosarcoma cells [9,11]. As for stimulation of biologic activities in bone cells, PDGF-BB is a potent stimulator and induces osteoblast proliferation and collagen synthesis [12]. It is recognized that PDGF, released during platelet aggregation, has a pivotal role in fracture healing as a systemic factor and that PDGF also regulates bone remodeling as a local factor [12]. Platelet-derived growth factor receptor has an intrinsic protein tyrosine kinase activity and associates with SH-2 domain–containing substrates such as phospholipase C-γ and phosphatidylinositol 3-kinase [9]. We have previously reported that PDGF-BB activates phosphatidylcholine-hydrolyzing phospholipase D via tyrosine kinase activation, resulting in protein kinase C activation in osteoblast-like MC3T3-E1 cells [13]. It has been shown that PDGF-BB induces the transcription of IL-6 through the activator protein 1 complex and activating transcription factor 2 in primary cultured rat osteoblasts [14]. However, the exact mechanism underlying PDGF-BB–stimulated IL-6 synthesis in osteoblasts is not fully known.

It is generally recognized that p70 S6 kinase is a mitogen-activated serine/threonine kinase required for cell

* Corresponding author. Tel.: +81 58 230 6214; fax: +81 58 230 6215.
E-mail address: okozawa@cc.gifu-u.ac.jp (O. Kozawa).

0026-0495/$ – see front matter © 2007 Elsevier Inc. All rights reserved.
doi:10.1016/j.metabol.2006.11.005

proliferation and G_1 cell-cycle progression [15]. As for osteoblasts, it has been shown that fluoroaluminate induces an increase in p70 S6 kinase phosphorylation [16]. In our previous study [17], we have reported that p70 S6 kinase plays as a positive regulator in bone morphogenetic protein 4–stimulated synthesis of vascular endothelial growth factor in osteoblast-like MC3T3-E1 cells. In addition, we recently demonstrated that p38 mitogen-activated protein (MAP) kinase, a member of the MAP kinase superfamily, functions at a point upstream from p70 S6 kinase in the synthesis of vascular endothelial growth factor in these cells [18]. However, the exact role of p70 S6 kinase in osteoblasts has not yet been fully clarified.

In the present study, we investigated the mechanism behind PDGF-BB–stimulated IL-6 synthesis in osteoblast-like MC3T3-E1 cells. We here show that PDGF-BB stimulates IL-6 synthesis through activation of 3 MAP kinases, p44/p42 MAP kinase, p38 MAP kinase, and stress-activated protein kinase/c-*Jun* N-terminal kinase (SAPK/JNK), in these cells, and that p70 S6 kinase concomitantly activated by PDGF-BB has an inhibitory role in the IL-6 synthesis.

2. Materials and methods

2.1. Materials

Platelet-derived growth factor–BB and mouse IL-6 and osteocalcin enzyme-linked immunosorbent assay (ELISA) kit were purchased from R&D Systems (Minneapolis, MN). Indomethacin was purchased from Sigma Chemical (St Louis, MO). PD98059, SB203580, SP600125, and rapamycin were obtained from Calbiochem-Novabiochem (La Jolla, CA). Phospho-specific p44/p42 MAP kinase antibodies, p44/p42 MAP kinase antibodies, phospho-specific p38 MAP kinase antibodies, p38 MAP kinase antibodies, phospho-specific SAPK/JNK antibodies, SAPK/JNK antibodies, phospho-specific p70 S6 kinase antibodies (Thr389), and p70 S6 kinase antibodies were purchased from Cell Signaling (Beverly, MA). ECL Western blotting detection system was purchased from Amersham Biosciences (Piscataway, NJ). Other materials and chemicals were obtained from commercial sources. PD98059, SB203580, SP600125, or rapamycin were dissolved in dimethyl sulfoxide. The maximum concentration of dimethyl sulfoxide was 0.1%, which did not affect the assay for IL-6 or Western blot analysis.

2.2. Cell culture

Cloned osteoblast-like MC3T3-E1 cells derived from newborn mouse calvaria [19] were maintained as previously described [20]. Briefly, the cells were cultured in α-minimum essential medium (α-MEM) containing 10% fetal calf serum (FCS) at 37°C in a humidified atmosphere of 5% CO_2/95% air. The cells were seeded into 35- or 90-mm diameter dishes in α-MEM containing 10% FCS. After 5 days, the medium was exchanged for α-MEM containing 0.3% FCS. The cells were used for experiments after 48 hours.

2.3. Interleukin 6 ELISA

The cultured cells were stimulated by various doses of PDGF-BB in 1 mL of α-MEM containing 0.3% FCS for the indicated periods. When indicated, the cells were pretreated

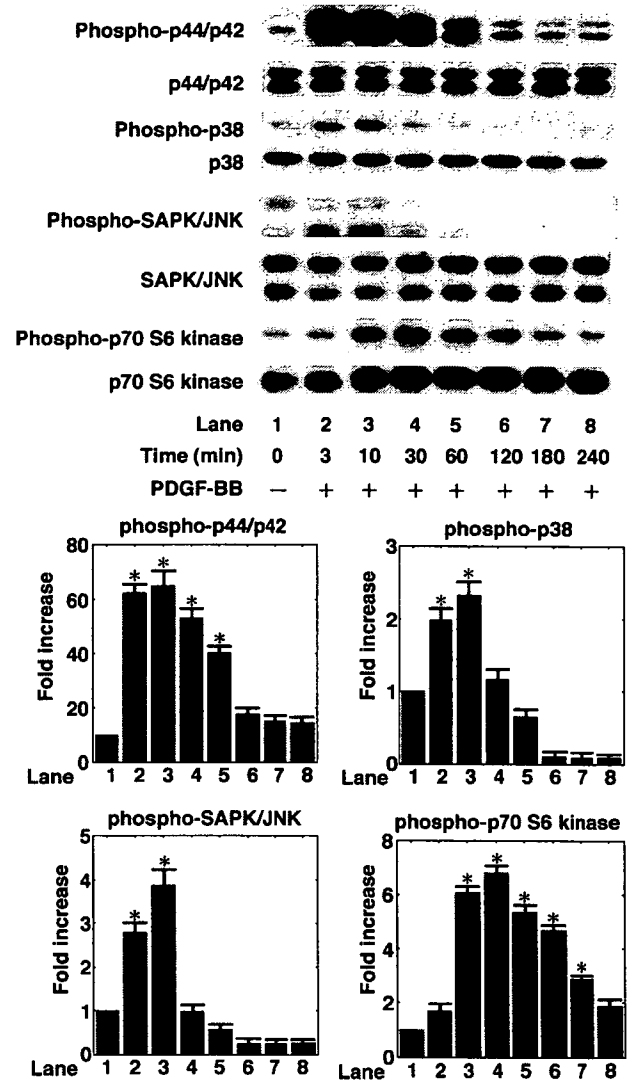

Fig. 1. Effects of PDGF-BB on the phosphorylation of p44/p42 MAP kinase, p38 MAP kinase, SAPK/JNK, or p70 S6 kinase in MC3T3-E1 cells. The cultured cells were stimulated by 50 ng/mL PDGF-BB for the indicated periods. The extracts of cells were subjected to sodium dodecyl sulfate-polyacrylamide gel electrophoresis with subsequent Western blotting analysis with antibodies against phospho-specific p44/p42 MAP kinase, p44/p42 MAP kinase, phospho-specific p38 MAP kinase, p38 MAP kinase, phospho-specific SAPK/JNK, SAPK/JNK, phospho-specific p70 S6 kinase, or p70 S6 kinase. Similar results were obtained with 2 additional and different cell preparations. The histogram shows quantitative representations of the levels of PDGF-BB–induced phosphorylation obtained from laser densitometric analysis of 3 independent experiments. Each value represents the mean ± SEM of triplicate determinations. Similar results were obtained with 2 additional and different cell preparations. $^*P < .05$ compared with the value of control.

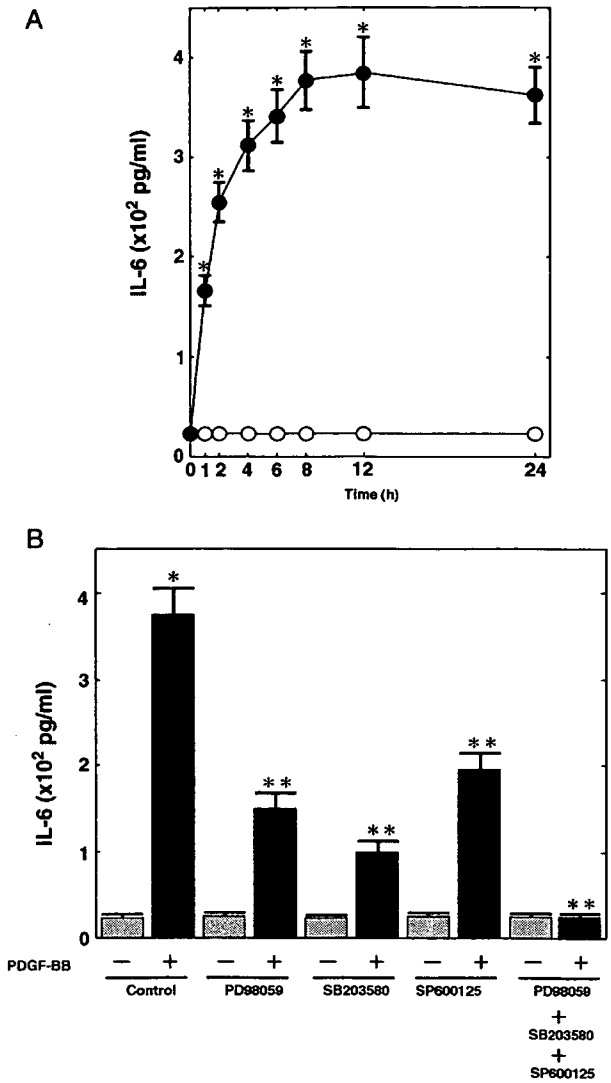

Fig. 2. Time course of PDGF-BB–induced IL-6 synthesis from MC3T3-E1 cells and effects of PD98059, SB203580, or SP600125 on the IL-6 synthesis by PDGF-BB in MC3T3-E1 cells. A, The cultured cells were stimulated by 50 ng/mL PDGF-BB (●) or vehicle (○) for the indicated periods. B, The cultured cells were pretreated with 3 μmol/L PD98059, 3 μmol/L SB203580, 3 μmol/L SP600125, or vehicle for 60 minutes and then stimulated by vehicle (gray bar) or 50 ng/mL PDGF-BB (black bar) for 24 hours. Each value represents the mean ± SEM of triplicate determinations. Similar results were obtained with 2 additional and different cell preparations. *$P < .05$ compared with the value of control. **$P < .05$ compared with the value of PDGF-BB alone.

with PD98059, SB203580, SP600125, indomathacin, or rapamycin for 60 minutes. The conditioned medium was collected at the end of the incubation, and the IL-6 concentration was measured by ELISA kit.

2.4. Osteocalcin ELISA

The cultured cells were pretreated with various doses of rapamycin for 60 minutes and then stimulated by 50 ng/mL PDGF-BB or vehicle for 24 hours. The conditioned medium was collected at the end of the incubation, and the osteocalcin concentration was measured by ELISA kit.

2.5. Western blot analysis

The cultured cells were stimulated by PDGF-BB in α-MEM containing 0.3% FCS for the indicated periods. The cells were washed twice with phosphate-buffered saline and then lysed, homogenized, and sonicated in a lysis buffer (pH 6.8) containing 62.5 mmol/L Tris/HCl, 2% sodium dodecyl sulfate, 50 mmol/L dithiothreitol, and 10% glycerol. The cytosolic fraction was collected as a supernatant after centrifugation at 125 000*g* for 10 minutes at 4°C. Sodium dodecyl sulfate-polyacrylamide gel electrophoresis was performed by Laemmli [21] in 10% polyacrylamide gel. Western blotting analysis was performed as described previously [22] by using phospho-specific p44/p42 MAP kinase antibodies, p44/p42 MAP kinase antibodies, phospho-specific p38 MAP kinase antibodies, p38 MAP kinase antibodies, phospho-specific SAPK/JNK antibodies, SAPK/JNK antibodies, phospho-specific p70 S6 kinase antibodies, or p70 S6 kinase antibodies, with peroxidase-labeled antibodies raised in goat-against-rabbit immunoglobulin G being used as second antibodies. Peroxidase activity on the polyvinylidene difluoride (PVDF) sheet was visualized on x-ray film by means of the ECL Western blotting detection system.

2.6. Determination

The absorbance of ELISA samples was measured at 450 nm with EL 340 Bio Kinetic Reader (Bio-Tek Instruments, Winooski, VT). The densitometric analysis was performed using Molecular Analyst/Macintosh (Bio-Rad Laboratories, Hercules, CA).

2.7. Statistical analysis

The data were analyzed by analysis of variance followed by the Bonferroni method for multiple comparisons between pairs, and $P < .05$ was considered significant. All data are presented as the mean ± SEM of triplicate determinations. Each experiment was repeated 3 times, with similar results.

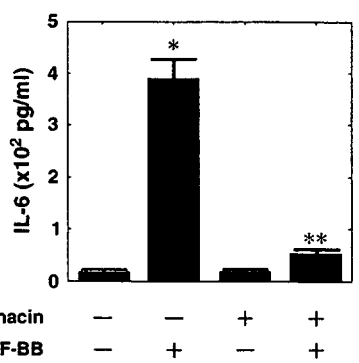

Fig. 3. Effect of indomethacin on the PDGF-BB–stimulated IL-6 synthesis in MC3T3-E1 cells. The cultured cells were pretreated with 10 μmol/L indomethacin or vehicle for 60 minutes and then stimulated by 50 ng/mL PDGF-BB or vehicle for 24 hours. Each value represents the mean ± SEM of triplicate determinations. Similar results were obtained with 2 additional and different cell preparations. *$P < .05$ compared with the control. **$P < .05$ compared with the value of PDGF-BB alone.

3. Results

3.1. Effects of PDGF-BB on the phosphorylation of p44/p42 MAP kinase, p38 MAP kinase, or SAPK/JNK in MC3T3-E1 cells

It is well recognized that 3 MAP kinases, p44/p42 MAP kinase, p38 MAP kinase, and SAPK/JNK, are known as central elements used by mammalian cells to transduce the various messages of a variety of agonists [23]. To investigate whether PDGF-BB activates MAP kinases in osteoblast-like MC3T3-E1 cells, we examined the effect of PDGF-BB on the phosphorylation of p44/p42 MAP kinase, p38 MAP kinase, or SAPK/JNK. Platelet-derived growth factor–BB time-dependently induced the phosphorylation of p44/p42 MAP kinase, p38 MAP kinase, and SAPK/JNK. The effect of PDGF-BB on the p44/p42 MAP kinase phosphorylation reached its peak at 10 minutes and continued to 60 minutes after the stimulation of PDGF-BB (Fig. 1). On the other hand, the effect on the phosphorylation of p38 MAP kinase reached its peak at 10 minutes and diminished within 30 minutes after the stimulation of PDGF-BB (Fig. 1). In addition, the maximum effect on the SAPK/JNK phosphorylation was observed at 10 minutes and diminished within 30 minutes after the stimulation of PDGF-BB (Fig. 1).

3.2. Effects of PD98059, SB203580, or SP600125 on the PDGF-BB–stimulated IL-6 synthesis in MC3T3-E1 cells

It has been reported that PDGF-BB induces IL-6 transcription in osteoblasts from fetal rat calvariae [14]. We found that PDGF-BB time-dependently stimulated IL-6 synthesis in osteoblast-like MC3T3-E1 cells (Fig. 2A). To clarify the involvement of the MAP kinase pathway in the PDGF-BB–stimulated IL-6 synthesis in these cells, we first examined the effect of PD98059, a specific inhibitor of MAP kinase/extracellular signal-regulated kinase kinase (MEK, an upstream kinase that activates p44/p42 MAP kinase) [24], on the IL-6 synthesis. PD98059, which by itself had little effect on the IL-6 levels, significantly suppressed the PDGF-BB–stimulated synthesis of IL-6 (Fig. 2B). Similarly, the IL-6 synthesis stimulated by PDGF-BB was markedly reduced by SB203580, a specific inhibitor of p38 MAP kinase [25], or SP600125, a specific SAPK/JNK inhibitor [26] (Fig. 2B). In addition, a combination of PD98059, SB203580, and SP600125 completely suppressed the PDGF-BB–stimulated synthesis of IL-6 (Fig. 2B). To determine whether these inhibitors themselves could affect cell survival, or cell number, the cell viability had been assessed by trypan blue dye exclusion test. We confirmed that the viability of the cells incubated at 37°C for 24 hours in the presence of 3 μmol/L PD980590, 3 μmol/L SB203580, or 3 μmol/L SP600125 was more than 90% compared with that of the control cells.

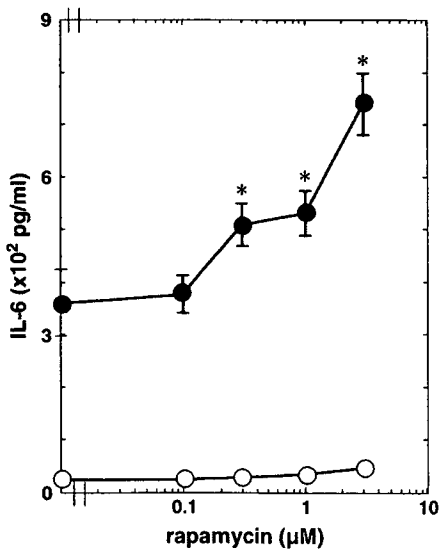

Fig. 4. Effect of rapamycin on the PDGF-BB–stimulated IL-6 synthesis in MC3T3-E1 cells. The cultured cells were pretreated with various doses of rapamycin for 60 minutes and then stimulated by 50 ng/mL PDGF-BB (●) or vehicle (○) for 24 hours. Each value represents the mean ± SEM of triplicate determinations. Similar results were obtained with 2 additional and different cell preparations. *$P < .05$ compared with the value of PDGF-BB alone.

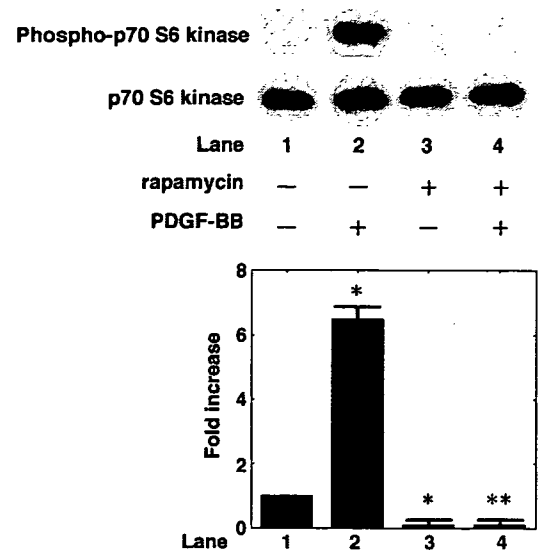

Fig. 5. Effect of rapamycin on the PDGF-BB–induced phosphorylation of p70 S6 kinase in MC3T3-E1 cells. The cultured cells were pretreated with 30 μmol/L rapamycin for 60 minutes and then stimulated by 50 ng/mL PDGF-BB or vehicle for 30 minutes. The extracts of cells were subjected to sodium dodecyl sulfate-polyacrylamide gel electrophoresis with subsequent Western blotting analysis with antibodies against phospho-specific p70 S6 kinase or p70 S6 kinase. The histogram shows quantitative representations of the levels of PDGF-BB–induced phosphorylation obtained from laser densitometric analysis of 3 independent experiments. Each value represents the mean ± SEM of triplicate determinations. Similar results were obtained with 2 additional and different cell preparations. *$P < .05$ compared with the value of control. **$P < .05$ compared with the value of PDGF-BB alone.

3.3. Effect of indomethacin on the PDGF-BB–stimulated IL-6 synthesis in MC3T3-E1 cells

Because we have previously reported that prostaglandins (PGs) increase IL-6 synthesis in MC3T3-E1 cells [27-30], to address whether endogenous PGs are involved in the

PDGF-BB–induced IL-6 synthesis in MC3T3-E1 cells, we examined the effect of indomethacin, an inhibitor of cyclooxygenase [31], on the IL-6 synthesis. Indomethacin, which by itself had no effect on the IL-6 levels, significantly reduced the PDGF-BB–induced synthesis of IL-6 (Fig. 3). These findings suggest that PGs mediate the stimulatory effect of PDGF-BB on IL-6 synthesis in these cells.

3.4. Effect of PDGF-BB on the phosphorylation of p70 S6 kinase in MC3T3-E1 cells

To clarify whether PDGF-BB activates p70 S6 kinase in MC3T3-E1 cells, we next examined the effect of PDGF-BB on the phosphorylation of p70 S6 kinase. p70 S6 kinase was time-dependently phosphorylated by PDGF-BB (Fig. 1). The maximum effect on the p70 S6 kinase phosphorylation was observed at 30 minutes after the stimulation of PDGF-BB, and the PDGF-BB effect continued 180 minutes after the stimulation.

3.5. Effect of rapamycin on the PDGF-BB–stimulated IL-6 synthesis in MC3T3-E1 cells

To investigate whether p70 S6 kinase is involved in the PDGF-BB–induced synthesis of IL-6 in MC3T3-E1 cells, we examined the effect of rapamycin, a specific inhibitor of p70 S6 kinase [32,33], on the synthesis of IL-6 induced by PDGF-BB. Rapamycin, which alone failed to affect the IL-6 levels, significantly enhanced the PDGF-BB–induced synthesis of IL-6 (Fig. 4). The amplifying effect of rapamycin was dose-dependent in the range between 0.1 and 3 μmol/L. Rapamycin at 3 μmol/L caused approximately 110% enhancement in the PDGF-BB effect.

3.6. Effect of rapamycin on the PDGF-BB–induced phosphorylation of p70 S6 kinase in MC3T3-E1 cells

We examined the effect of rapamycin on the PDGF-BB–induced phosphorylation of p70 S6 kinase. Rapamycin, which itself significantly suppressed the phosphorylation of p70 S6 kinase in itself, truly suppressed the PDGF-BB–induced phosphorylation of p70 S6 kinase (Fig. 5).

3.7. Effect of rapamycin on the proliferation or the differentiation of MC3T3-E1 cells

To determine whether rapamycin could affect cell survival, or cell number, the cell viability had been assessed by trypan blue dye exclusion test. We confirmed that the viability of the cells incubated at 37°C for 24 hours in the

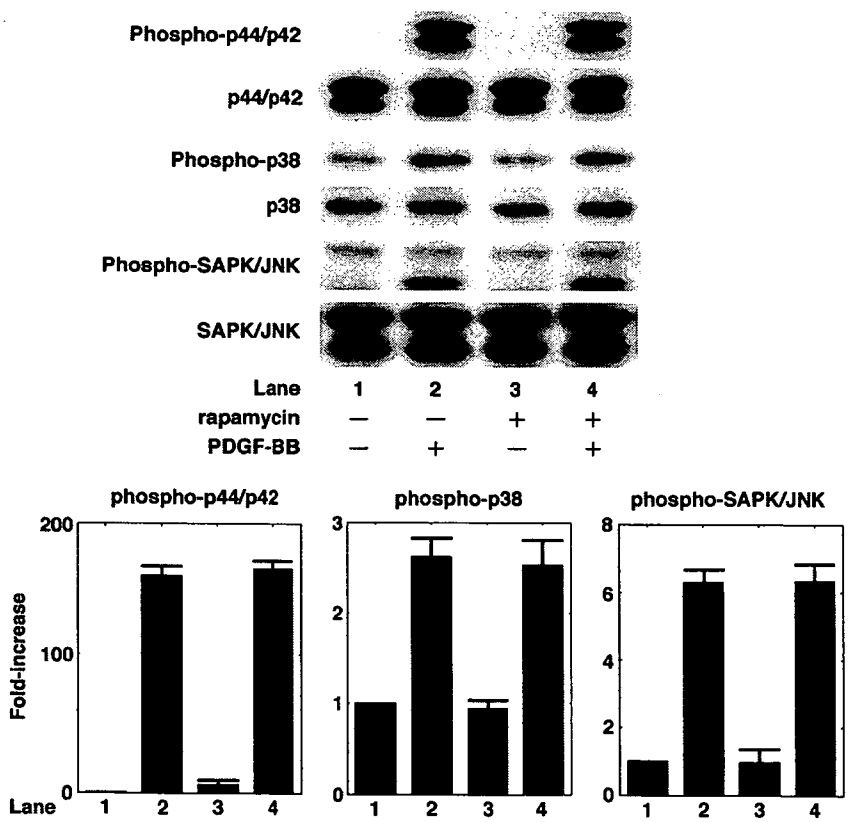

Fig. 6. Effects of rapamycin on the PDGF-BB–induced phosphorylation of p44/p42 MAP kinase, p38 MAP kinase, or SAPK/JNK in MC3T3-E1 cells. The cultured cells were pretreated with 30 μmol/L rapamycin or vehicle for 60 minutes and then stimulated by 50 ng/mL PDGF-BB or vehicle for 10 minutes. The extracts of cells were subjected to sodium dodecyl sulfate-polyacrylamide gel electrophoresis with subsequent Western blotting analysis with antibodies against phospho-specific p44/p42 MAP kinase, p44/p42 MAP kinase, phospho-specific p38 MAP kinase, p38 MAP kinase, phospho-specific SAPK/JNK, or SAPK/JNK. The histogram shows quantitative representations of the levels of PDGF-BB–induced phosphorylation obtained from laser densitometric analysis of 3 independent experiments. Each value represents the mean ± SEM of triplicate determinations. Similar results were obtained with 2 additional and different cell preparations.

presence of 3 μmol/L rapamycin was more than 90% compared with that of the control cells. To determine whether rapamycin could affect the cell proliferation, we counted the cell number before and after the 24-hour incubation with rapamycin. We confirmed that rapamycin did not affect the cell number at a dose of 3 μmol/L ($9.7 \pm 1.1 \times 10^5$ cells/mL for control; $15.6 \pm 1.6 \times 10^5$ cells/mL for 50 ng/mL PDGF-BB alone; $10.1 \pm 1.4 \times 10^5$ cells/mL for 3 μmol/L rapamycin alone; and $14.7 \pm 1.6 \times 10^5$ cells/mL for 50 ng/mL PDGF-BB with 3 μmol/L rapamycin, as measured during the stimulation for 24 hours).

Next, to determine whether rapamycin affects the differentiation of these cells, we examined the effect of rapamycin on the production of osteocalcin, a mature osteoblast phenotype [34], in MC3T3-E1 cells. Platelet-derived growth factor–BB or rapamycin did not induce osteocalcin production in MC3T3-E1 cells (2.7 ± 0.3 ng/mL for control; 2.6 ± 0.3 ng/mL for 50 ng/mL PDGF-BB alone; 2.5 ± 0.4 ng/mL for 3 μmol/L rapamycin alone; and 2.5 ± 0.3 ng/mL for 50 ng/mL PDGF-BB with 3 μmol/L rapamycin, as measured during the stimulation for 24 hours). These findings as a whole suggest that rapamycin hardly affects the proliferation and the differentiation of osteoblast-like MC3T3-E1 cells within 24 hours.

3.8. Effects of rapamycin on the PDGF-BB–induced phosphorylation of p44/p42 MAP kinase, p38 MAP kinase, or SAPK/JNK in MC3T3-E1 cells

To investigate whether rapamycin's effect on the PDGF-BB–stimulated IL-6 synthesis is dependent on the activation of p44/p42 MAP kinase, p38 MAP kinase, or SAPK/JNK, we next examined the effect of rapamycin on the phosphorylation of p44/p42 MAP kinase, p38 MAP kinase, or SAPK/JNK induced by PDGF-BB in these cells. However, rapamycin failed to affect the PDGF-BB–induced phosphorylation of p44/p42 MAP kinase, p38 MAP kinase, or SAPK/JNK (Fig. 6).

4. Discussion

In the present study, we found that PDGF-BB time-dependently induced the phosphorylation of p70 S6 kinase in osteoblast-like MC3T3-E1 cells, using phospho-specific p70 S6 kinase (Thr389) antibodies. It is generally recognized that the activity of p70 S6 kinase is regulated by multiple phosphorylation events [15]. It has been shown that phosphorylation at Thr389 most strongly correlates with p70 S6 kinase activity [15]. Taking these results into account, it is most likely that PDGF-BB activates p70 S6 kinase in osteoblast-like MC3T3-E1 cells. To the best of our knowledge, this is probably the first report showing the PDGF-BB–induced p70 S6 kinase activation in osteoblasts.

We next demonstrated that PDGF-BB induces the phosphorylation of p44/p42 MAP kinase, p38 MAP kinase, and SAPK/JNK in these cells. It is well recognized that the MAP kinase superfamily mediates intracellular signaling of extracellular agonists and plays an important role in cellular functions including proliferation, differentiation, and apoptosis in a variety of cells [23]. Three major MAP kinases, p44/p42 MAP kinase, p38 MAP kinase, and SAPK/JNK, are known as central elements used by mammalian cells to transduce diverse messages [23]. It has been shown that MAP kinases are activated by phosphorylation of threonine and tyrosine residues by dual-specificity MAP kinases [23]. Therefore, our findings strongly suggest that PDGF-BB activates 3 MAP kinases, p44/p42 MAP kinase, p38 MAP kinase, and SAPK/JNK, in osteoblast-like MC3T3-E1 cells. In addition, we showed that the PDGF-BB–stimulated IL-6 synthesis was suppressed by a MEK inhibitor, PD98059 [24]; a specific p38 MAP kinase inhibitor, SB203580 [25]; or a specific SAPK/JNK inhibitor, SP600125 [26], in these cells. Thus, it is probable that PDGF-BB stimulates the synthesis of IL-6 via the 3 MAP kinases in osteoblast-like MC3T3-E1 cells. We have previously reported that PGs increase IL-6 synthesis in MC3T3-E1 cells [27-30]. In the present study, we found that indomethacin significantly reduced the PDGF-BB–induced synthesis of IL-6. These results suggest that PDGF-BB–induced IL-6 production is mediated, at least in part, by PDGF-BB–stimulated PG production in osteoblast-like MC3T3-E1 cells. In addition, we have previously shown that PGE_2, a major product of eicosanoids in osteoblasts, significantly stimulates IL-6 synthesis after 3 hours in MC3T3-E1 cells [30]. On the contrary, PDGF-BB significantly stimulated the IL-6 production within 3 hours. Taking our findings into account, it is quite likely that there will be PG-dependent and PG-independent effects of PDGF-BB–stimulated IL-6 synthesis, as has been demonstrated for so many growth factors and cytokines in bone cells, and it would be important to be define these. Therefore, experiments using PGE_2 itself instead of PDGF-BB are required.

We investigated whether p70 S6 kinase functions in the PDGF-BB–stimulated IL-6 synthesis in osteoblast-like MC3T3-E1 cells. The PDGF-BB–stimulated synthesis of IL-6 was significantly amplified by rapamycin, a specific inhibitor of p70 S6 kinase [31,32]. We confirmed that rapamycin truly suppressed the PDGF-BB–induced phosphorylation of p70 S6 kinase. It seems that the activated p70 S6 kinase plays an inhibitory role in the IL-6 synthesis by PDGF-BB in osteoblast-like MC3T3-E1 cells. Therefore, taking our results into account, it is most likely that PDGF-BB activates p70 S6 kinase, resulting in down-regulation of IL-6 synthesis. It is probable that the p70 S6 kinase signaling pathway activated by PDGF-BB limits the PDGF-BB–stimulated IL-6 synthesis. As far as we know, our present finding is probably the first report to show that the activation of p70 S6 kinase leads to the negative-feedback regulation of IL-6 synthesis in osteoblasts.

We investigated the relationship between p70 S6 kinase and 3 MAP kinases in the PDGF-BB–stimulated IL-6 synthesis in MC3T3-E1 cells. However, rapamycin failed to enhance the PDGF-BB–induced phosphorylation levels of

p44/p42 MAP kinase, p38 MAP kinase, and SAPK/JNK. Therefore, it seems unlikely that p70 S6 kinase signaling pathway affects the PDGF-BB–stimulated synthesis of IL-6 through the amplification of activities of 3 MAP kinases, p44/p42 MAP kinase, p38 MAP kinase, and SAPK/JNK, in osteoblast-like MC3T3-E1 cells.

The p70 S6 kinase pathway is recognized to play a crucial role in various cellular functions, especially cell-cycle progression [15]. Our present results indicate that the p70 S6 kinase pathway in osteoblasts has an important role in the control of the production of IL-6, one of the key regulators of bone metabolism. It is well known that IL-6 produced by osteoblasts is a potent bone resorptive agent and induces osteoclast formation [3,4]. The mitogenic activities of PDGF-BB and its release by platelets suggest an important role in wound healing and fracture repair [35]. It is also possible that PDGF-BB plays a role in acute bone repair after inflammation because the mitogenic actions of PDGF-BB are enhanced in the presence of cytokines [35]. Therefore, our present findings lead us to speculate that PDGF-BB–activated p70 S6 kinase acts as a negative regulator of bone resorption through the fine tuning of the local cytokine network. Thus, the p70 S6 kinase pathway in osteoblasts might be considered to be a new candidate as a molecular target of bone resorption concurrent with various bone diseases. On the contrary, we have previously shown that p70 S6 kinase acts as a positive regulator in bone morphogenetic protein-4–stimulated synthesis of vascular endothelial growth factor in MC3T3-E1 cells [17]. The physiologic significance of regulatory mechanism by p70 S6 kinase in osteoblasts still remains unclear. Further investigation is required to clarify the exact role of p70 S6 kinase in osteoblasts.

In conclusion, our results strongly suggest that p70 S6 kinase plays an important role in the regulation of PDGF-BB–stimulated, MAP kinase–mediated IL-6 synthesis in osteoblasts and may serve as a negative feedback mechanism to prevent from oversynthesizing IL-6 in these cells.

Acknowledgments

This investigation was supported in part by Grant-in-Aid for Scientific Research (16590873 and 16591482) from the Ministry of Education, Science, Sports and Culture of Japan, Research Grants for Longevity Sciences (15A-1 and 15C-2), and by the Research on Proteomics and the Research on Fracture and Dementia from the Ministry of Health, Labour and Welfare of Japan.

We are very grateful to Yoko Kawamura and Seiko Sakakibara for their skillful technical assistance.

References

[1] Akira S, Taga T, Kishimoto T. Interleukin-6 in biology and medicine. Adv Immunol 1993;54:1-78.

[2] Heymann D, Rousselle AV. gp130 Cytokine family and bone cells. Cytokine 2000;12:1455-68.

[3] Kwan Tat S, Padrines M, Theoleyre S, Heymann D, Fortun Y. IL-6 is produced by osteoblasts and induces bone resorption. Cytokine Growth Factor Rev 2004;15:49-60.

[4] Nijweide PJ, Burger EH, Feyen JHM. Cells of bone: proliferation, differentiation, and hormonal regulation. Physiol Rev 1986; 86:855-86.

[5] Ishimi Y, Miyaura C, Jin CH, Akatsu T, Abe E, Nakamura Y, et al. IL-6 is produced by osteoblasts and induces bone resorption. J mmunol 1990;145:3297-303.

[6] Roodman GD. Interleukin-6: an osteotropic factor? J Bone Miner Res 1992;7:475-8.

[7] Helle M, Brakenhoff JPJ, DeGroot ER, Aarden LA. Interleukin 6 is involved in interleukin 1–induced activities. Eur J Immunol 1998; 18:957-9.

[8] Littlewood AJ, Russil J, Harvey GR, Hughes DE, Russel RGG, Gowen M. The modulation of the expression of IL-6 and its receptor in human osteoblasts in vitro. Endocrinology 1991;129:1513-20.

[9] Heldin CH, Westermark B. Mechanism of action and in vivo role of platelet-derived growth factor. Physiol Rev 1999;79:1283-316.

[10] Heldin CH, Eriksson U, Ostman A. New members of the platelet-derived growth factor family of mitogens. Arch Biochem Biophys 2002;398:284-90.

[11] Heldin CH, Johnsson A, Wennergren S, Wernstedt C, Betsholtz C, Westermark B. A human osteosarcoma cell line secretes a growth factor structurally related to a homodimer of PDGF A-chains. Nature 1986;319:511-4.

[12] Canalis E, Varghese S, McCarthy TL, Centrella M. Role of platelet derived growth factor in bone cell function. Growth Regul 1992;2:151-5.

[13] Kozawa O, Suzuki A, Watanabe Y, Shinoda J, Oiso Y. Effect of platelet-derived growth factor on phosphatidylcholine-hydrolyzing phospholipase D in osteoblast-like cells. Endocrinology 1995; 136:4473-8.

[14] Franchimont N, Durant D, Rydziel S, Canalis E. Platelet-derived growth factor induces interleukin-6 transcription in osteoblasts through the activator protein–1 complex and activating transcription factor–2. J Biol Chem 1999;274:6783-9.

[15] Pullen N, Thomas G. The modular phosphorylation and activation of p70s6k. FEBS Lett 1997;410:78-82.

[16] Susa M, Standke GJ, Jeschke M, Rohner D. Fluoroaluminate induces pertussis toxin-sensitive protein phosphorylation: differences in MC3T3-E1 osteoblastic and NIH3T3 fibroblastic cells. Biochem Biophys Res Commun 1997;235:680-4.

[17] Kozawa O, Matsuno H, Uematsu T. Involvement of p70 S6 kinase in bone morphogenetic protein signaling: vascular endothelial growth factor synthesis by bone morphogenetic protein-4 in osteoblasts. J Cell Biochem 2001;81:430-6.

[18] Tokuda H, Hatakeyama D, Shibata T, Akamatsu S, Oiso Y, Kozawa O. p38 MAP kinase regulates BMP-4–stimulated VEGF synthesis via p70 S6 kinase in osteoblasts. Am J Physiol Endocrinol Metab 2003; 284:E1202-9.

[19] Sudo H, Kodama H, Amagai Y, Yamamoto S, Kasai S. In vitro differentiation and calcification in a new clonal osteogenic cell line derived from newborn mouse calvaria. J Cell Biol 1983;96:191-8.

[20] Kozawa O, Tokuda H, Miwa M, Kotoyori J, Oiso Y. Cross-talk regulation between cyclic AMP production and phosphoinositide hydrolysis induced by prostaglandin E2 in osteoblast-like cells. Exp Cell Res 1992;198:130-4.

[21] Laemmli UK. Cleavage of structural proteins during the assembly of the head of bacteriophage T4. Nature 1970;227:680-5.

[22] Kato K, Ito H, Hasegawa K, Inaguma Y, Kozawa O, Asano T. Modulation of the stress-induced synthesis of hsp27 and alpha B-crystallin by cyclic AMP in C6 rat glioma cells. J Neurochem 1996;66:946-50.

[23] Widmann C, Gibson S, Jarpe MB, Johnson GL. Mitogen-activated protein kinase: conservation of a three-kinase module from yeast to human. Physiol Rev 1999;79:143-80.

[24] Alessi DR, Cuenda A, Cohen P, Dudley DT, Saltiel AR. PD98059 is a specific inhibitor of the activation of mitogen-activated protein kinase in vitro and in vivo. J Biol Chem 1995;270:27489-94.
[25] Cuenda A, Rouse J, Doza YN, Meier R, Cohen P, Gallagher TF, Young PR, Lee JC. SB203580 is a specific inhibitor of a MAP kinase homologue which is stimulated by cellular stresses and interleukin-1. FEBS Lett 1995;364:229-33.
[26] Bennett BL, Sasaki DT, Murray BW, O'Leary EC, Sakata ST, Xu W, et al. SP600125, an anthrapyrazolone inhibitor of Jun N-terminal kinase. Proc Natl Acad Sci U S A 2001;98:13681-6.
[27] Watanabe-Tomita Y, Suzuki A, Oiso Y, Kozawa O. Prostaglandin E1 stimulates interleukin-6 secretion via protein kinase A in osteoblast-like cells. Cell Signal 1997;9:105-8.
[28] Kozawa O, Suzuki A, Tokuda H, Uematsu T. Prostaglandin F2alpha stimulates interleukin-6 synthesis via activation of PKC in osteoblast-like cells. Am J Physiol 1997;272:E208-11.
[29] Tokuda H, Kozawa O, Harada A, Uematsu T. Prostaglandin D2 induces interleukin-6 synthesis via Ca2+ mobilization in osteoblasts: regulation by protein kinase C. Prostaglandins Leukot Essent Fatty Acids 1999;61:189-94.
[30] Kozawa O, Suzuki A, Tokuda H, Kaida T, Uematsu T. Interleukin-6 induced by prostaglandin E2: cross-talk regulation by protein kinase C. Bone 1998;22:355-60.
[31] Smith WL. The eicosanoids and their biochemical mechanisms of action. Biochem J 1989;259:315-24.
[32] Price DJ, Grove JR, Calvo V, Avruch J, Bierer BE. Rapamycin-induced inhibition of the 70-kilodalton S6 protein kinase. Science 1992;257:973-7.
[33] Kuo CJ, Chung J, Fiorentino DF, Flanagan WM, Blenis J, Crabtree GR. Rapamycin selectively inhibits interleukin-2 activation of p70 S6 kinase. Nature 1992;358:70-3.
[34] Ducy P, Desbois C, Boyce C, Pinero G, Story B, Dunstan C, et al. Increased bone formation in osteocalcin-deficient mice. Nature 1996;382:448-52.
[35] Canalis E, Rydziel S. Platelet-derived growth factor and the skeleton. In: Belizikian J, Raisz LJ, Rodan G, editors. Principles of Bone Biology. 2nd ed. San Diego: Academic Press; 2002. p. 817-24.

Available online at www.sciencedirect.com
ScienceDirect
Analytical Biochemistry 364 (2007) 37–50
ANALYTICAL BIOCHEMISTRY
www.elsevier.com/locate/yabio

Novel fucogangliosides found in human colon adenocarcinoma tissues by means of glycomic analysis

Hiroaki Korekane [a,b], Satoyo Tsuji [a], Shingo Noura [c], Masayuki Ohue [c], Yo Sasaki [c], Shingi Imaoka [c], Yasuhide Miyamoto [a,*]

[a] *Department of Immunology, Osaka Medical Center for Cancer and Cardiovascular Diseases, 1-3-2 Nakamichi, Higashinari-ku, Osaka 537-8511, Japan*
[b] *Japan Health Science Foundation, 13-4 Nihonbashi Kodenma-cho, Chuo-ku, Tokyo 103-0001, Japan*
[c] *Department of Surgery, Osaka Medical Center for Cancer and Cardiovascular Diseases, 1-3-3 Nakamichi, Higashinari-ku, Osaka 537-8511, Japan*

Received 29 November 2006
Available online 31 January 2007

Abstract

The structures of acidic glycosphingolipids in colon adenocarcinoma have been analyzed extensively using a number of conventional methods, such as thin-layer chromatography and methylation analysis, and a variety of acidic glycosphingolipids present in the tissues have been reported. However, because of a number of limitations in the techniques used in previous studies in terms of resolution, quantification, and sensitivity, we employed a different method that could be applied to small amounts of tissue. In this technique, the carbohydrate moieties of acidic glycosphingolipids from approximately 20 mg of colon adenocarcinoma were released by endoglycoceramidase II and were labeled by pyridylamination. They were separated and structurally characterized by a two-dimensional HPLC mapping technique, electrospray ionization tandem mass spectrometry (ESI–MS/MS), and enzymatic cleavage. A total of 22 major acidic glycosphingolipid structures were identified, and their relative quantities were revealed in detail. They are composed of 1 sulfated (SM3), 1 lacto-series (SLe^a), 6 kinds of ganglio-series, and 14 kinds of neolacto-series glycosphingolipids. They include most of the acidic glycosphingolipids previously reported to be present in the tissues and two previously unknown fucogangliosides sharing the same terminal structure: NeuAcα2-6(Fucα1-2)Galβ1-4GlcNAcβ1-3Galβ1-4Glc, and NeuAcα2-6(Fucα1-2)Galβ1-4GlcNAcβ1-3Galβ1-4(Fucα1-3)GlcNAcβ1-3-Galβ1-4Glc. Thus, this highly sensitive, high-resolution analysis enabled the identification of novel structures of acidic glycosphingolipids from small amounts of already comprehensively studied cancerous tissues. This method is a powerful tool for microanalysis of glycosphingolipid structures from small quantities of cancerous tissues and should be applicable to different types of malignant tissues.

Keywords: Ganglioside; Colon cancer; Structure; Pyridylamination; Mass spectrometry; Two-dimensional mapping

* Corresponding author. Fax: +81 6 6972 7749.
E-mail address: miyamoto-ya@mc.pref.osaka.jp (Y. Miyamoto).

0003-2697/$ - see front matter © 2007 Elsevier Inc. All rights reserved.
doi:10.1016/j.ab.2007.01.034

Alterations in glycosphingolipid (GSL)[1] compositions on the cell surface of tumors occur in essentially all types of human cancers [1]. Extensive studies have been performed to analyze the structure of GSLs from a variety of tumor tissues [2–7]. Furthermore, a series of GSLs unusually accumulated in cancerous tissues have been successfully isolated and characterized [8–11] and reveal that each type of tumor is characterized by accumulation of specific types of GSLs. For example, unusual accumulations of GSLs having type 1 or 2 chain derivatives (i.e., those with Le^a, Le^x, Le^y, or dimeric Le^x and their sialosyl derivatives) are observed in most human adenocarcinoma [9,11–13], whereas GD3 is observed in melanoma [3]. However, due to a number of limitations of the techniques used, these analyses may be lacking in terms of identification and quantification. In general, in the techniques applied previously, GSLs extracted from cancerous tissues were separated by HPLC using organic solvents and traditional thin-layer chromatography (TLC) methodology where resolved GSLs were stained with orcinol. A single band on TLC might not ensure homogeneity, and separation of GSLs having similar mobility on TLC sometimes may be difficult even though a variety of separation solvents are used [13]. Hence, it is possible that certain GSLs having similar chromatographic behavior on TLC were not separated to homogeneity and escaped detection even in well-studied cancerous tissues. Furthermore, although quantification of each GSL is important to better understand the precise features of glycosylation of cancerous tissue, the quantities of individual GSLs in cancer tissues have not been well defined because quantification by scanning densitometry of orcinol-stained bands on TLC is limited by the severe restriction in the linear range due to variation in band size or geometry following migration. Thus, more detailed analyses of GSL structures in cancerous tissues using improved methodology that overcomes the limitations described above may be required, even in tissues already well studied.

Here we employ a powerful methodology to analyze the structures of GSLs from small quantities of colon adenocarcinoma (~ 20 mg). The techniques are highly sensitive and capable of separating the major GSLs and analyzing them quantitatively as well as qualitatively [14]. The methodology employs the use of endoglycoceramidase to release the carbohydrate moieties of GSLs, fluorescent labeling with 2-aminopyridine, and HPLC analysis. Furthermore, each GSL could be identified by a two-dimensional (2-D) mapping technique together with electrospray ionization–tandem mass spectrometry (ESI–MS/MS).

Colon adenocarcinoma is one of the most widely examined tissues in terms of the structures of GSLs of cancerous tissues [2,8–13,15] and was used as the source of material in this study to allow us to evaluate the effectiveness of the new techniques through comparison with results reported previously.

In this study, we focus on the acidic GSLs among the GSLs and elucidate the fine structures of major acidic GSLs present in colonic adenocarcinoma tissues more precisely than reported previously. In particular, we describe the structure of novel fucosyl gangliosides.

Materials and methods

Isolation of acidic GSLs from colon adenocarcinoma tissues

All patients had undergone simultaneous resections of primary colon tumors and liver metastases at Osaka Medical Center for Cancer and Cardiovascular Diseases (Osaka, Japan). Fresh cancerous tissues were frozen with liquid nitrogen and stored at –80 °C until use. The samples were cut to a thickness of 10 μm with a cryostat microtome. A total of 20 sections were collected, homogenized in 10 ml of chloroform/methanol (2:1, v/v), and stored for 2 h at room temperature with 30 s of sonication every 30 min. Then 5 ml of methanol was added, and the sample was centrifuged at 1800 *g* for 15 min. The pellets were homogenized in 10 ml of chloroform/methanol/water (1:2:0.8, v/v/v), stored for 2 h at room temperature, and centrifuged at 1800 *g* for 15 min. Both extracts were combined and evaporated to dryness in a vacuum concentrator. The residue was dissolved in chloroform/methanol/water (30:60:8) and fractionated by DEAE–Sephadex A25 column chromatography into neutral and acidic GSLs.

Preparation of acidic pyridylaminated oligosaccharides

The acidic GSLs were digested at 37 °C for 16 h with 10 mU of recombinant endoglycoceramidase II from *Rhodococcus* sp. (Takara Bio, Shiga, Japan) in 50 μl of 0.1 M sodium acetate (pH 5.0) containing 0.1% taurodeoxycholate [16]. Released oligosaccharides were labeled with 2-aminopyridine (2-AP), and excess reagent was removed by phenol/chloroform extraction [17,18].

[1] *Abbreviations used:* GSL, glycosphingolipid; GD3, Neu5Acα8Neu5Acα3Galβ-4GlcCer; TLC, thin-layer chromatography; 2-D, two-dimensional; ESI–MS/MS, electrospray ionization–tandem mass spectrometry; 2-AP, 2-aminopyridine; PA, pyridylaminated; Gu, glucose units; RP, reversed phase; CID, collision-induced dissociation; asialo GM2, GalNAcβ4Galβ4Glc; asialo GM1, Galβ3GalNAcβ4Galβ4Glc; GM3, Neu5Acα3Galβ4Glc; GM2, GalNAcβ4(Neu5Acα3)Galβ4Glc; GD1a, Neu5Acα3Galβ3GalNAcβ4(Neu5Acα3)Galβ4Glc; GD1b, Galβ3GalNAcβ4(Neu5Acα8Neu5Acα3)Galβ4Glc; GT1b, Neu5Acα3Galβ3GalNAcβ4(Neu5Acα8Neu5Acα3)Galβ4Glc; GQ1b, Neu5Acα8Neu5Acα3Galβ3GalNAcβ4(Neu5Acα8Neu5Acα3)Galβ4Glc; globotriose, Galα4Galβ4Glc; Le^b-hexasaccharide, Fucα2Galβ3(Fucα4)GlcNAcβ3Galβ4Glc; A-hexasaccharide, GalNAcα3(Fucα2)Galβ3GlcNAcβ3Galβ4Glc; A-heptasaccharide, GalNAcα3(Fucα2)Galβ3(Fucα4)GlcNAcβ3Galβ4Glc; 2-fucosyllactose, Fucα2Galβ4Glc; A-tetrasaccharide, GalNAcα3(Fucα2)Galβ4Glc; SM2,GalNAcβ4(HSO^3)3Galβ4GlcCer; SM3, $HSO^3$3Galβ4GlcCer; H^1, Fucα2Galβ4GlcNAcβ3Galβ4Glc; Lc^4, Galβ3GlcNAcβ3Galβ4Glc; nLc^4, Galβ4GlcNAcβ3Galβ4Glc; Cer, ceramide; LST-c, Neu5Acα6Galβ4GlcNAcβ3Galβ4Glc; SPG, sialyl-paragloboside, Neu5Acα3Galβ4GlcNAcβ3Galβ4Glc; LST-a, Neu5Acα3Galβ3GlcNAcβ3Galβ4Glc; SLex, sialyl-Lewis X, Neu5Acα3Galβ4(Fucα3)GlcNAcβ3Galβ4GlcCer.

HPLC for pyridylaminated-oligosaccharides separation

Pyridylaminated (PA)-oligosaccharides were separated on a Shimazu LC-20A HPLC system equipped with a Waters 2475 fluorescence detector. Size fractionation HPLC was performed on a TSK gel Amide-80 column (0.2 × 25 cm, Tosoh, Tokyo, Japan) at 40 °C at a flow rate of 0.2 ml/min using two solvents: A and B. Solvent A was acetonitrile/0.5 M acetic acid containing 10% acetonitrile, adjusted to pH 7.3 with triethylamine (75:15, v/v). Solvent B was acetonitrile/0.5 M acetic acid containing 10% acetonitrile, adjusted to pH 7.3 with triethylamine (40:50, v/v). The column was equilibrated with solvent A. After injection of sample, the proportion of solvent B was programmed to increase from 0 to 100% in 100 min. The PA-oligosaccharides were detected by fluorescence with an excitation wavelength of 310 nm and an emission wavelength of 380 nm. The molecular size of each PA-oligosaccharide is given in glucose units (Gu) based on the elution times of PA-isomaltooligosaccharides. Reversed phase (RP)–HPLC was performed on a TSK gel ODS-80Ts column (0.2×15 cm, Tosoh) at 30 °C at a flow rate of 0.2 ml/min using two solvents: C and D. Solvent C was 50 mM acetic acid, adjusted to pH 6.0 with triethylamine. Solvent D was 50 mM acetic acid containing 20% acetonitrile, adjusted to pH 6.0 with triethylamine. The column was equilibrated with solvent C. After injection of sample, the proportion of solvent D was programmed to increase from 0 to 18% in 54 min. The PA-oligosaccharides were detected by excitation at 315 nm and emission at 400 nm. The retention time of each PA-oligosaccharide is given in glucose units based on the elution times of PA-isomaltooligosaccharides. Thus, a given compound from these two columns provided a unique set of Gu (amide) and Gu (ODS) values that correspond to coordinates of the 2-D map. When coordinates are cited in this article, they are listed in the order of Gu (ODS), Gu (amide).

Glycosidase digestion

Sialyl PA-oligosaccharides were digested with 2 U/ml of α2,3-sialidase from *Salmonella typhimurium* (Takara Bio) or 2 U/ml α-sialidase from *Arthrobacter ureafaciens* (Nacalai, Kyoto, Japan) in 100 mM sodium acetate buffer (pH 5.5) for 2 h at 37 °C (condition 1). Under these conditions, α2,3-sialidase specifically digests sialic acid α2-3 linked to the terminal residue but not sialic acid with a α2-6 linkage, whereas *Arthrobacter* α-sialidase digests both linkages independent of the linkage position. However, under conditions using 10 U/ml for 16 h (condition 2), even so-called α2,3-sialidase can hydrolyze sialic acid α2-6 linked to the terminal residue but not sialic acid linked to a nonterminal residue. Hence, we were able to conclude the linkage position of sialic acid using these two enzymes as follows. First, when sialyl PA-oligosaccharide was cleaved by α2,3-sialidase in condition 1, sialic acid was concluded to be linked to the terminal residue through an α2-3 linkage. Second, when sialyl PA-oligosaccharide was cleaved by α2,3-sialidase in condition 2 but not in condition 1, sialic acid was concluded to be linked to the terminal residue through an α2-6 linkage. Third, when sialyl PA-oligosaccharide was cleaved by *Arthrobacter* α-sialidase in condition 1 but not by α2,3-sialidase even in condition 2, sialic acid was concluded to be linked to a nonterminal residue. The enzyme specificity was demonstrated using the following model substrates: NeuAcα2-3Galβ1-4Glc-NAcβ1-3Galβ1-4Glc-PA (sialylparagloboside), NeuAcα2-6Galβ1-4GlcNAcβ1-3Galβ1-4Glc-PA (LS-tetrasaccharide *c*), Galβ1-3(NeuAcα2-6)GlcNAcβ1-3Galβ1-4Glc-PA (LS-tetrasaccharide *b*), and Galβ1-3GalNAcβ1-4(NeuAcα2-3)Galβ1-4Glc-PA (GM1).

In other glycosidase digests, PA-oligosaccharides were digested with (i) 0.2 mU/ml of α1,3/4-fucosidase from *Streptomyces* sp. 142 (Takara Bio) in 100 mM sodium acetate buffer (pH 5.5) for 2 h at 37 °C, (ii) 0.4 U/ml β1,4-galactosidase from *Streptococcus pneumonia* (Prozyme, San Leandro, CA, USA) in 100 mM sodium citrate buffer (pH 6.0) for 2 h at 37 °C, (iii) 10 U/ml of β-*N*-acetylhexosaminidase from jack bean (Seikagaku Kogyo, Tokyo, Japan) in 100 mM sodium citrate buffer (pH 5.0) for 16 h at 37 °C, (iv) 4 U/ml of α1,2-fucosidase from *Corynebacterium* sp. (Takara Bio) in 100 mM sodium phosphate buffer (pH 8.5), (v) 0.5 U/ml of endo-β-galactosidase from *Escherichia freundii* (Seikagaku Kogyo) in 100 mM sodium acetate buffer (pH 5.8) for 16 h at 37 °C, and (vi) 10 U/ml of α-fucosidase from bovine kidney (Sigma, St. Louis, MO, USA) in 100 mM sodium acetate buffer (pH 5.8) for 16 h at 37 °C. All of the reactions were terminated by boiling the solutions for 3 min at 100 °C.

Electrospray ionization MS^n

PA-oligosaccharides were analyzed by LC/ESI–MS/MS. HPLC was performed on a Paradigm MS4 equipped with a Magic C18 column (0.2 × 50 mm, Michrome BioResource, Auburn, CA, USA). Each PA-oligosaccharide was injected with a flow rate of 2 μl/min for 3 min and eluted with 50% methanol for 10 min.

MS analyses were performed using an LCQ ion trap mass spectrometer (Thermo Finnigan, San Jose, CA, USA) equipped with a nano-electrospray ion source (AMR, Tokyo, Japan). The nanospray voltage was set to 1.8 kV in the positive ion mode. The heated desolvation capillary temperature was set to 180 °C. In the LCQ method file, the LCQ was set to acquire a full MS scan between *m/z* 400 and 2000 followed by MS/MS or MS/MS/MS scans in a data-dependent manner. Relative collision energy for collision-induced dissociation (CID) was set to 30% with a 30-ms activation time for MS^2 and MS^3 experiments. MS^2 and MS^3 were performed with an isolation width of 4.0 u (range of precursor ion ± 2.0). Protonated ions were subjected to a further product ion scan for nonfucosylated PA-oligosaccharides. However, sodiated ions were subjected to a further product ion scan for

fucose-containing PA-oligosaccharides because intramolecular fucose rearrangements have been found in the CID spectra of protonated ions (but not in sodiated ions) produced from oligosaccharides derivatized at their reducing termini with aromatic amines, such as 2-aminobenzamide, which may lead to erroneous conclusions about oligosaccharide sequence [19].

Standard PA-oligosaccharides

Standard PA-oligosaccharides, including PA-lactose, PA-asialo GM2, PA-asialo GM1, PA-GM3, PA-GM2, PA-GM1, PA-GD1a, PA-GD1 b, PA-GD3, PA-GT1b, PA-GQ1b, PA-globotriose, PA-globotetraose, PA-Forssman pentsaccharide, PA-lactoneotetraose, PA-lactotetraose, PA-lactofucopentaose I, PA-lactofucopentaose II, PA-lactofucopentaose III, PA-Le^b-hexasaccharide, PA-A-hexasaccharide, PA-A-heptasaccharide, PA-2-fucosyllactose, and PA-A-tetrasaccharide, were purchased from Takara Bio. Glycolipids SM2 and SM3 were kindly donated by Koichi Honke (Kochi University Medical School). Sialylated Le^x glycolipid was purchased from Wako Pure Chemicals (Tokyo, Japan). Oligosaccharides, including LS-tetrasaccharide *a*, LS-tetrasaccharide *b*, and LS-tetrasaccharide *c*, were purchased from Prozyme, and Lewis Y hexasaccharide was purchased from Sigma. SM3, SM2, sialylated Le^x, LS-tetrasaccharide *a*, LS-tetrasaccharide *b*, LS-tetrasaccharide *c*, and Lewis Y hexasaccharide were pyridylaminated as described above. PA-H_1 was obtained from PA-Lewis Y hexasaccharide by releasing the fucosyl residue linked to the third GlcNAc by α1,3/4-fucosidase digestion. PA-sialylparagloboside was prepared from human erythrocytes using the following procedure. Acidic GSLs were extracted from 3 ml of human erythrocytes, pyridylaminated, and resolved by size fractionation HPLC as described above. Sialylparagloboside was most abundant in acidic GSLs of erythrocytes. Fractions corresponding to PA-sialylparagloboside were collected and further purified by RP–HPLC. The structure of PA-sialylparagloboside was unambiguously confirmed by enzymatic digestion and MS. GlcNAcβ1-3Galβ1-4Glc-PA and GlcNAcβ1-3Galβ1-4GlcNAcβ1-3Galβ1-4Glc-PA were prepared as standard compounds for endo-β-galactosidase treatment by digestion of PA-nLc_4 and PA-nLc_6, respectively, with β1,4-galactosidase (see Results). Although 2-D mapping techniques have been widely used for the analysis of structures of *N*-glycans, the technique seldom has been applied to the analysis of structures of GSLs. Hence, prior to analysis of cancerous tissues, we evaluated the potential of the method by analyzing all of the PA-oligosaccharides prepared in this study, including 16 acidic and 18 neutral oligosaccharides, by HPLC using the two types of column (ODS and amide). All of the PA-oligosaccharides except PA-lactofucopentaose II (Le^a) and PA-lactofucopentaose III (Le^x) were clearly separated on the map under the chromatographic conditions used in this study (data not shown). PA-Le^a and PA-Le^x could be discriminated following α1,3/4-fucosidase digestion because the digestion products, namely PA-lactotetraose (Lc_4) and PA-lactoneotetraose (nLc_4), elute at positions with distinct glucose units on both columns (Table 1). Hence, we concluded that the 2-D mapping technique was also applicable for the analysis of structures of GSLs. The structures, abbreviations, and glucose units of authentic PA-oligosaccharides used in this study are listed in Table 1.

Results

Preparation and separation of acidic PA-oligosaccharides from colon adenocarcinoma

Acidic GSLs from three cases of primary colonic adenocarcinoma and hepatic metastasis were extracted. Acidic glycans from the ceramide (Cer) moieties were released by endoglycoceramidase II treatment. Efficiency of release of glycans from the ceramide moiety by endoglycoceramidase II has been reported to be greater than 95% [20]. To detect sugars with high sensitivity, the reducing ends of the released oligosaccharides were tagged with the fluorophore 2-AP. Qualitatively similar, but quantitatively slightly different, chromatographic profiles of acidic PA-oligosaccharides were obtained from six samples: the primary colon cancer and liver metastatic deposits from three patients. In this article, we show the most representative data from the liver metastatic deposit of one particular patient. The acidic PA-oligosaccharides from a liver metastatic deposit of a colon adenocarcinoma were analyzed by size fractionation HPLC in which separation depends on the molecular size of the oligosaccharides (Fig. 1). A total of 17 peaks (G1–G17) were obtained (Fig. 1), with each peak being further purified by RP–HPLC. Peaks G10, G14, and G17 were separated into two major components, and G16 was separated into three major components, each designated G10-1, G10-2, G14-1, G14-2, G16-1, G16-2, G16-3, G17-1, and G17-2, in RP–HPLC. In addition, purified acidic PA-oligosaccharides were subjected to LC/ESI–MS/MS, where product ion spectra of the precursor ions were acquired data-dependently. Peaks marked by an open arrowhead in Fig. 1 contained neutral PA-oligosaccharides, as determined by MS analyses. This probably is due to desialylation of PA-oligosaccharides during the process of pyridylamination. Elution positions of G1 to G17-2 on size fractionation and RP–HPLC are summarized in Fig. 2 as a 2-D map.

Structure of G1 to G9

From comparison of the positions on the map with the positions of standard acidic PA-oligosaccharides, G1, G2, G3, G4, G5, G7, G8 and G9 are predicted to be SM3, GM3, GM2, GD3, GM1, GD1a, LST-c, and GD1b, respectively. Strong candidates for the identity of G6 are

Table 1
Structures and elution positions in HPLC of standard PA-oligosaccharides

Abbreviation	Structure	Elution position in HPLC	
		Size (Gu)	RP (Gu)
SM3	HSO_3-Galβ1-4Glc-PA	1.19	2.60
GM3	Neu5Acα2-3Galβ1-4Glc-PA	2.46	3.00
GM2	GalNAcβ1-4Galβ1-4Glc-PA 3 Neu5Acα2	2.97	3.01
GM1	Galβ1-3GalNAcβ1-4Galβ1-4Glc-PA 3 Neu5Acα2	3.85	2.92
GD3	Neu5Acα2-8Neu5Acα2-3Galβ1-4Glc-PA	3.31	4.50
GD1a	Galβ1-3GalNAcβ1-4Galβ1-4Glc-PA 3 3 Neu5Acα2 Neu5Acα2	4.10	5.03
GD1b	Galβ1-3GalNAcβ1-4Galβ1-4Glc-PA 3 Neu5Acα2-8Neu5Acα2	4.64	3.96
SPG	Neu5Acα2-3Galβ1-4GlcNAcβ1-3Galβ1-4Glc-PA	4.02	4.52
LST-a	Neu5Acα2-3Galβ1-3GlcNAcβ1-3Galβ1-4Glc-PA	4.01	4.69
LST-c	Neu5Acα2-6Galβ1-4GlcNAcβ1-3Galβ1-4Glc-PA	4.40	3.76
SLe^x	Neu5Acα2-3Galβ1-4GlcNAcβ1-3Galβ1-4Glc-PA 3 Fucα1	4.75	4.08
Lc_4	Galβ1-3GlcNAcβ1-3Galβ1-4Glc-PA	3.66	2.50
nLc_4	Galβ1-4GlcNAcβ1-3Galβ1-4Glc-PA	3.74	2.16
H_1	Fucα1-2Galβ1-4GlcNAcβ1-3Galβ1-4Glc-PA	4.15	3.80
LFP II (Le^a)	Galβ1-3GlcNAcβ1-3Galβ1-4Glc-PA 4 Fucα1	4.51	2.01
LFP III (Le^x)	Galβ1-4GlcNAcβ1-3Galβ1-4Glc-PA 3 Fucα1	4.51	1.99

SPG and LST-a (Fig. 2). After α2,3-sialidase digestion, G6 was converted to nLc_4 but not Lc_4, indicating that G6 is SPG. The structures of G1 to G9 were also confirmed by MS/MS. Fractions eluting later than G9 on the amide column, with the exception of G10-1, do not match any of the reference compounds on the 2-D map (Fig. 2). In the following sections, the structures of acidic PA-oligosaccharides with the same monosaccharide compositions are explained in detail. Elution positions, mass data, and estimated composition of G10-1 to G17-2 are presented in Table 2.

Structure of G10-1, G10-2, and G11

G10-1 and G11 were digested with α2,3-sialidase in conditions in which this enzyme specifically cleaves the α2,3 linkage (condition 1). The products of both digests corresponded to either Le^a or Le^x on the map (thick-line and thin-line arrows in Fig. 3). The desialylated products from G10-1 and G11 were digested with α1,3/4-fucosidase, and the positions of the products of the digests corresponded to nLc_4 and Lc_4, respectively. These results suggest that the structure of G10-1 is SLe^x and the structure of G11 is

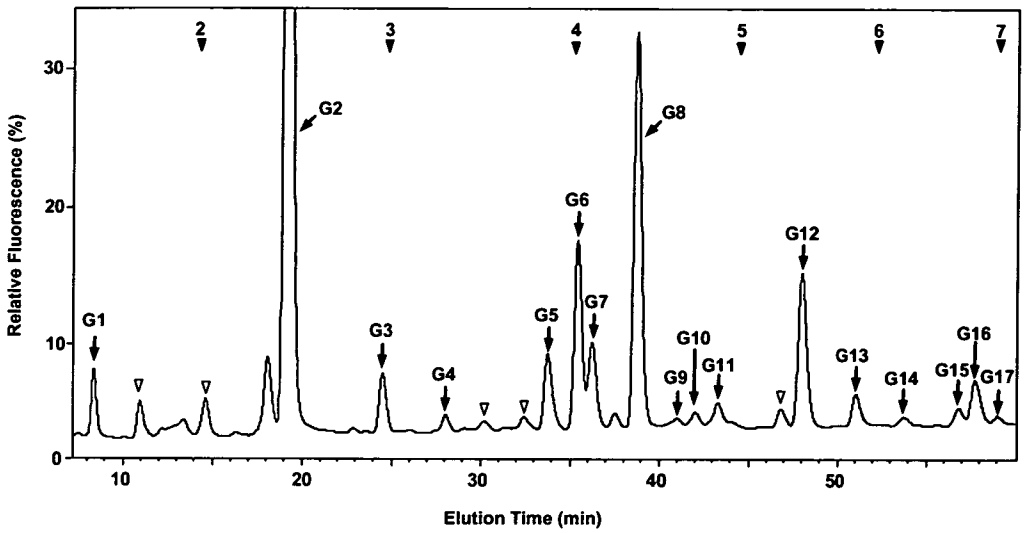

Fig. 1. Elution profile of the acidic PA-oligosaccharide mixtures obtained from colon adenocarcinoma tissue on the amide column. Relative fluorescence of the highest peak, G2, was set to 100%. A total of 17 peaks, which are predicted to be acidic PA-oligosaccharides by MS analysis, are termed G1 to G17 and highlighted with arrows. Numbered closed arrowheads indicate the elution positions of PA-isomaltooligosaccharides with the corresponding degree of polymerization. The peaks marked by the open arrowheads contained neutral PA-oligosaccharides.

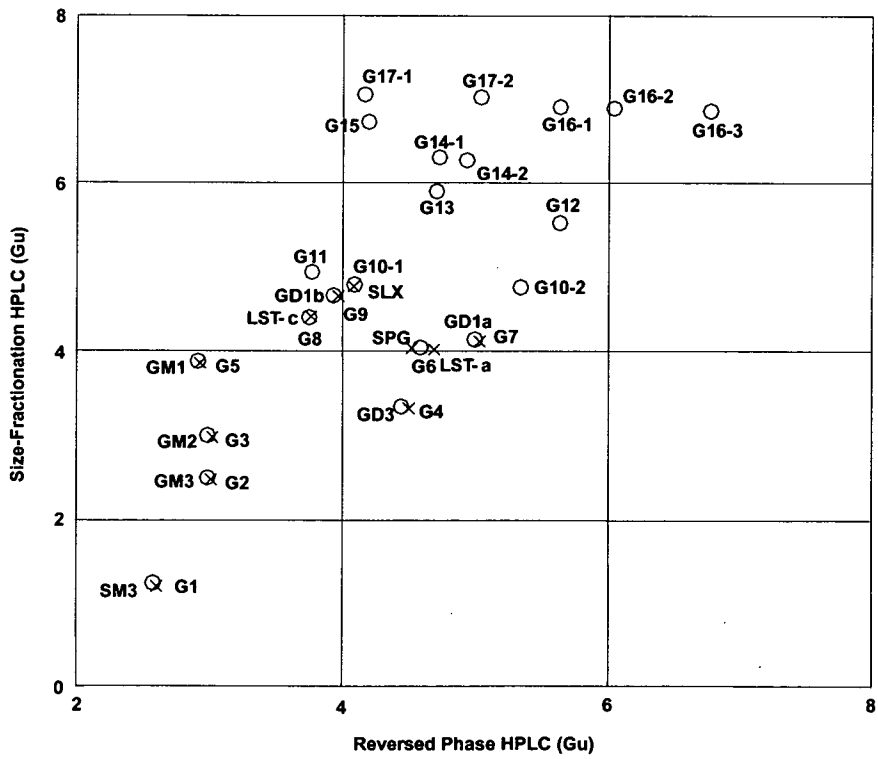

Fig. 2. Two-dimensional map of acidic PA-oligosaccharides. The elution positions of each acidic PA-oligosaccharide on the size fractionation and RP–HPLC are expressed in glucose units based on the elution times of the PA-isomaltooligosaccharides and plotted on the map. Circles indicate the positions of the acidic PA-oligosaccharides from colon adenocarcinoma tissue. Xs indicate the positions of the standard acidic PA-oligosaccharides.

SLe[a] (Table 3). These structures are consistent with the structures deduced by MS/MS analysis (Fig. 4, right, with only MS^{1-3} spectra of G11 shown in the figure). In contrast to G10-1 and G11, G10-2 could not be digested with α2,3-sialidase in the conditions where this enzyme specifically cleaves the α2-3 linkage (condition 1) but could be digested with α2,3-sialidase in the conditions where this enzyme cleaves the α2-3 and α2-6 linkages (condition 2). These

Table 2
Elution positions in HPLC and mass analysis of acidic PA-oligosaccharides from colon adenocarcinoma tissue eluted later than G9 on the amide column

Fraction	Elution position in HPLC		Mass (observed)	Mass (calculated)	Estimated composition
	Size (Gu)	RP (Gu)			
G10-1	4.78	4.09	1223.5	1223.5 $[M+H]^+$	$NeuAc_1Hex_3HexNAc_1dHex_1$-PA
G10-2	4.74	5.35	1223.5	1223.5 $[M+H]^+$	$NeuAc_1Hex_3HexNAc_1dHex_1$-PA
G11	4.92	3.77	1223.3	1223.5 $[M+H]^+$	$NeuAc_1Hex_3HexNAc_1dHex_1$-PA
G12	5.51	5.64	1442.4	1442.5 $[M+H]^+$	$NeuAc_1Hex_4HexNAc_2$-PA
G13	5.89	4.71	1442.6	1442.5 $[M+H]^+$	$NeuAc_1Hex_4HexNAc_2$-PA
G14-1	6.29	4.73	1588.4	1588.6 $[M+H]^+$	$NeuAc_1Hex_4HexNAc_2dHex_1$-PA
G14-2	6.25	4.94	1588.3	1588.6 $[M+H]^+$	$NeuAc_1Hex_4HexNAc_2dHex_1$-PA
G15	6.71	4.19	1588.4	1588.6 $[M+H]^+$	$NeuAc_1Hex_4HexNAc_2dHex_1$-PA
G16-1	6.90	5.64	1807.1	1807.7 $[M+H]^+$	$NeuAc_1Hex_5HexNAc_3$-PA
G16-2	6.87	6.05	1807.4	1807.7 $[M+H]^+$	$NeuAc_1Hex_5HexNAc_3$-PA
G16-3	6.85	6.78	1807.5	1807.7 $[M+H]^+$	$NeuAc_1Hex_5HexNAc_3$-PA
G17-1	7.04	4.16	1734.4	1734.7 $[M+H]^+$	$NeuAc_1Hex_4HexNAc_2dHex_2$-PA
G17-2	7.00	5.04	1734.3	1734.7 $[M+H]^+$	$NeuAc_1Hex_4HexNAc_2dHex_2$-PA

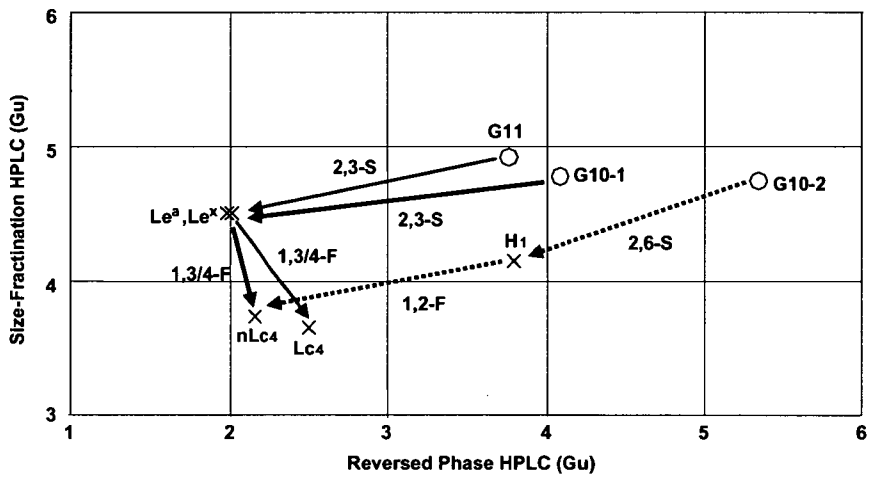

Fig. 3. Sequential digestion of PA-oligosaccharides G10-1, G10-2, and G11. Circles indicate the positions of G10-1, G10-2, and G11. Thick-line, dotted-line, and thin-line arrows indicate the directions of the changes after glycosidase digestion of G10-1, G10-2, and G11, respectively. Glycosidases are shown beside each line. Enzyme abbreviations: 2,3-S, α2,3-sialidase under conditions where the enzyme specifically digests sialic acid in the α2-3 linkage; 2,6-S, α2,3-sialidase under conditions where the enzyme digests sialic acid in both α2-3 and α2-6 linkages; 1,3/4-F, α1,3/4-fucosidase; 1,2-F, α1,2 fucosidase. Xs mark the positions of the standard compounds.

results suggest that sialic acid is α2-6 linked to the terminal residue (see Materials and Methods). In addition, the desialylated product of G10-2 corresponded to H_1 on the 2-D map (dashed-line arrows in Fig. 3). After desialylation, G10-2 could be digested with α1,2-fucosidase but not with α1,3/4-fucosidase, and the position of the product of the digest on the map corresponded with that of nLc_4. On the basis of these data, G10-2 is estimated to be NeuAcα2-6(Fucα1-2)Galβ1-4GlcNAcβ1-3Galβ1-4Glc, a structure that has not been reported previously (Table 3). These structures are consistent with the results from MS/MS analysis (Fig. 4, left). The mass spectrum of MS^3 of G10-2 revealed it to have a core tetrasaccharide structure: Hex-HexNAc-Hex-Hex-PA. The presence of a fragment ion at *m/z* 534, corresponding to $[dHex+Hex-HexNAc+Na]^+$ in the MS^3 spectra of G10-2, indicates that a fucosyl residue is linked to the outermost Hex or HexNAc residue. However, the characteristic product ion at *m/z* 792, corresponding to $[dHex-HexNAc-Hex-Hex-PA+Na]^+$, was observed in the MS^3 spectrum of G10-1 and G11 (Fig. 4, right) but not in the MS^3 spectra of G10-2, suggesting that a fucosyl residue is linked to the outermost Hex residue but not the HexNAc residue in G10-2.

Structure of G12 and G13

G12 was digested successfully with α2,3-sialidase in condition 1. In contrast, G13 could not be digested with α2,3-sialidase under the same conditions, but could be digested in condition 2. Both desialylation products had very similar behavior on the HPLC eluting at the same positions (2.93, 5.38), indicating that G12 and G13 have the same structural backbone and that sialic acid is linked α2-3 and α2-6, respectively, to the terminal residue. Desialylated products from G12 and G13 were sequentially digested

Table 3
Estimated structures of acidic PA-oligosaccharides from colonic adenocarcinoma

Fraction	Structure	Abbreviation	Ratio (%)
G1	HSO_3-Galβ1-4Glc-PA	SM3	1.6
G2	Neu5Acα2-3Galβ1-4Glc-PA	GM3	58.0
G3	GalNAcβ1-4Galβ1-4Glc-PA 3 Neu5Acα2	GM2	1.9
G4	Neu5Acα2-8Neu5Acα2-3Galβ1-4Glc-PA	GD3	0.6
G5	Galβ1-3GalNAcβ1-4Galβ1-4Glc-PA 3 Neu5Acα2	GM1	2.8
G6	Neu5Acα2-3Galβ1-4GlcNAcβ1-3Galβ1-4Glc-PA	SPG	6.5
G7	Galβ1-3GalNAcβ1-4Galβ1-4Glc-PA 3 3 Neu5Acα2 Neu5Acα2	GD1a	2.9
G8	Neu5Acα2-6Galβ1-4GlcNAcβ1-3Galβ1-4Glc-PA	IV ^{6}NeuAcα-nLc$_4$	13.8
G9	Galβ1-3GalNAcβ1-4Galβ1-4Glc-PA 3 Neu5Acα2-8Neu5Acα2	GD1b	0.2
G10-1	Neu5Acα2-3Galβ1-4GlcNAcβ1-3Galβ1-4Glc-PA 3 Fucα1	SLe^x	0.4
G10-2	Neu5Acα2-6Galβ1-4GlcNAcβ1-3Galβ1-4Glc-PA 2 Fucα1	IV^{2}Fucα,IV^{6}NeuAcα-nLc$_4$	0.2
G11	Neu5Acα2-3Galβ1-3GlcNAcβ1-3Galβ1-4Glc-PA 4 Fucα1	SLe^a	1.3
G12	Neu5Acα2-3Galβ1-4GlcNAcβ1-3Galβ1-4GlcNAcβ1-3Galβ1-4Glc-PA	VI^{3}NeuAcα-nLc$_6$	6.0
G13	Neu5Acα2-6Galβ1-4GlcNAcβ1-3Galβ1-4GlcNAcβ1-3Galβ1-4Glc-PA	VI^{6}NeuAcα-nLc$_6$	1.2
G14-1	Neu5Acα2-3Galβ1-4GlcNAcβ1-3Galβ1-4GlcNAcβ1-3Galβ1-4Glc-PA 3 Fucα1	VI^{3}NeuAcα,III^{3}Fucα-nLc$_6$	0.1
G14-2	Neu5Acα2-3Galβ1-4GlcNAcβ1-3Galβ1-4GlcNAcβ1-3Galβ1-4Glc-PA 3 Fucα1	VI^{3}NeuAcα,V^{3}Fucα-nLc$_6$	0.1
G15	Neu5Acα2-6Galβ1-4GlcNAcβ1-3Galβ1-4GlcNAcβ1-3Galβ1-4Glc-PA 3 Fucα1	VI^{6}NeuAcα,III^3 Fucα-nLc$_6$	0.7
G16-1	Neu5Acα2-3Galβ1-4HexNAc Galβ1-4GlcNAcβ1-3Galβ1-4Glc-PA 3 Galβ1-4GlcNAcβ1		0.1
G16-2	Galβ1-4HexNAc Galβ1-4GlcNAcβ1-3Galβ1-4Glc-PA 3 Neu5Acα2-3Galβ1-4GlcNAcβ1		0.2
G16-3	Neu5Acα2-3Galβ1-4GlcNAcβ1-(3Galβ1-4GlcNAcβ1)$_2$-3Galβ1-4Glc-PA	VIII^{3}NeuAcα-nLc$_8$	1.0
G17-1	Neu5Acα2-3Galβ1-4GlcNAcβ1-3Galβ1-4GlcNAcβ1-3Galβ1-4Glc-PA 3 3 Fucα1 Fucα1	VI^{3}NeuAcα,V^{3}Fucα,III^{3}Fucα-nLc$_6$	0.2
G17-2	Neu5Acα2-6Galβ1-4GlcNAcβ1-3Galβ1-4GlcNAcβ1-3Galβ1-4Glc-PA 2 3 Fucα1 Fucα1	VI^{2}Fucα,VI^{6}NeuAcα,III^{3}Fucα-nLc$_6$	0.1

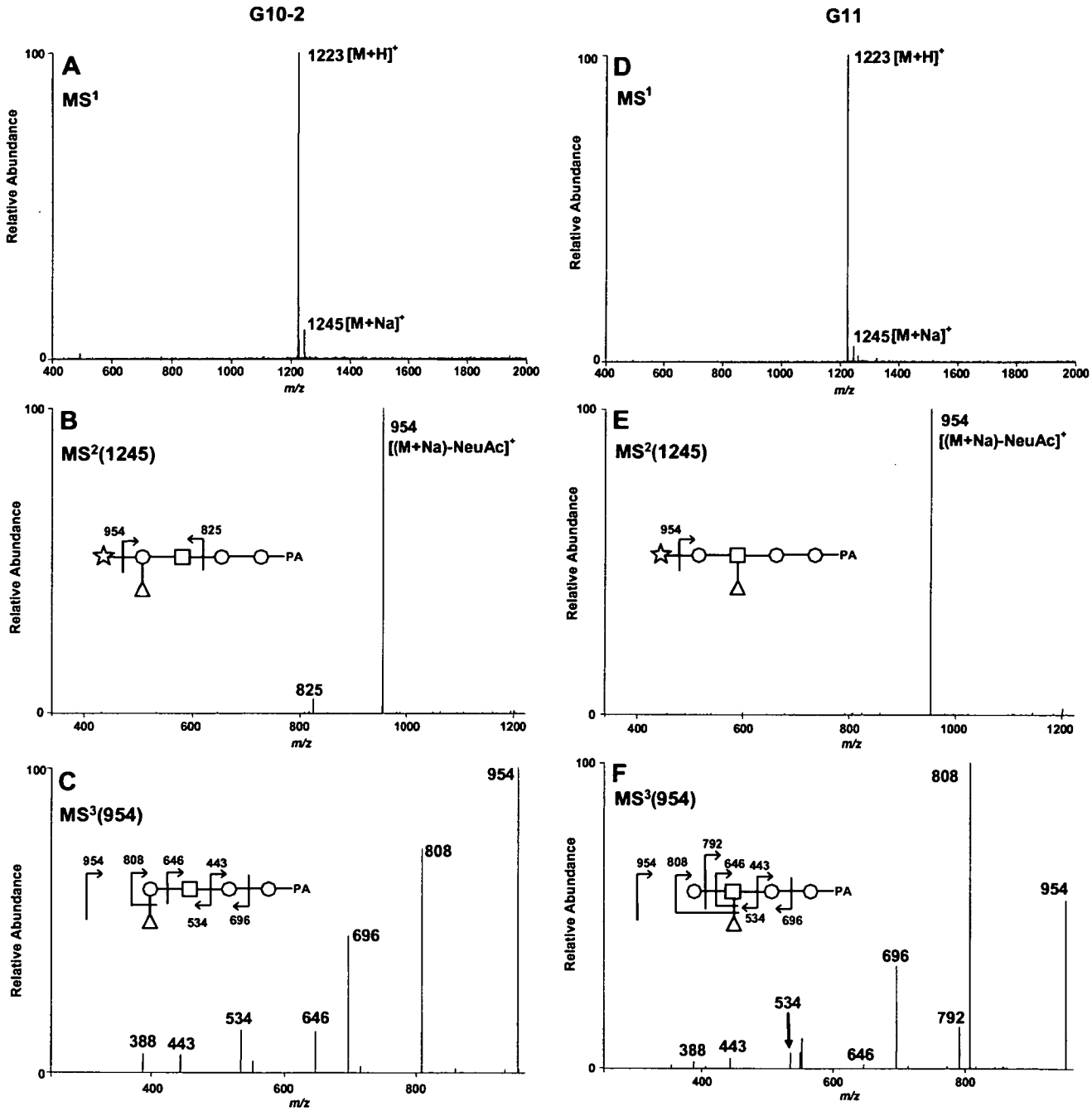

Fig. 4. MS^{1-3} spectra of G10-2 and G11. (A,D) MS^1 spectra of G10-2 (A) and G11 (D). (B,E) MS^2 spectra of $[M+Na]^+$ precursor ion at *m/z* 1245 detected in MS^1 of panel A (B) and panel D (E). (C,F) MS^3 spectra of $[(M+Na)\text{-NeuAc}]^+$ precursor ion at *m/z* 954 detected in MS^2 of panel B (C) and panel E (F). Fragment ions numbered mass values in panels B, C, E, and F are sodium adduct ions. The MS/MS fragment ions were assigned as shown schematically. Symbols: open circle, Hex; open square, HexNAc; open star, sialic acid; open triangle, dHex.

with β1,4-galactosidase and β-*N*-acetylhexosaminidase. The products of both digests corresponded to nLc_4 on the map, indicating the structure of both backbones to be Galβ1-4HexNAc-Galβ1-4GlcNAcβ1-3Galβ1-4Glc. Hydrolysis of G12 and G13 with endo-β-galactosidase gave two peaks by HPLC, corresponding Glc-PA and GlcNAcβ1-3Galβ1-4Glc-PA. These results indicate that the subterminal HexNAc is GlcNAc linked β1-3 to galactose. Hence, the structures of G12 and G13 are estimated to be as shown in Table 3. These structures are consistent with tandem mass analysis data (data not shown).

Structure of G14-1, G14-2, and G15

Sialic acid is linked α2-3 to the terminal residue of G14-1 and G14-2 and linked α2-6 to terminal residue